NASA CONTRACTOR REPORT

ULTRASONIC ATTENUATION AND VELOCITY MEASUREMENTS IN THE NORMAL AND SUPERCONDUCTING STATES OF NIOBIUM

by J. Trivisonno, J. Washick, M. J. Keck, R. Reifenberger, and T. Slotwinski

Prepared by
JOHN CARROLL UNIVERSITY
University Heights, Ohio
for Lewis Research Center

NATIONAL AERONAUTICS AND SPACE ADMINISTRATION • WASHINGTON, D. C. • JANUARY 1971

1. Report No.	2. Government Accession No.	3. Recipient's Catalog No.
NASA CR-1742		

4. Title and Subtitle	5. Report Date
ULTRASONIC ATTENUATION AND VELOCITY MEASUREMENTS IN THE NORMAL AND SUPERCONDUCTING STATES OF NIOBIUM	January 1971
	6. Performing Organization Code

7. Author(s)	8. Performing Organization Report No.
J. Trivisonno, J. Washick, M. J. Keck, R. Reifenberger, and T. Slotwinski	None
	10. Work Unit No.
9. Performing Organization Name and Address	
John Carroll University University Heights, Ohio	11. Contract or Grant No. NGR 36-006-003
	13. Type of Report and Period Covered
12. Sponsoring Agency Name and Address	Contractor Report
National Aeronautics and Space Administration Washington, D. C. 20546	14. Sponsoring Agency Code

15. Supplementary Notes

16. Abstract

Ultrasonic attenuation measurements in niobium single crystals at frequencies from 50 to 810 MHz over the temperature range 3.0 to 11.0^{o} K are presented. The attenuation in superconducting niobium is found to differ from the behavior predicted by the BCS theory for both longitudinal and transverse modes. A ql dependence is found for longitudinal waves but not for transverse waves. Ultrasonic measurements in the mixed state of niobium as a function of orientation are presented. The mixed state attenuation of longitudinal and transverse waves is found to be in qualitative agreement with the predictions of the Maki-Kinder theory. A system used to measure changes in the ultrasonic velocity with a sensitivity of 1 part in 10^{7} is presented. Changes in the velocity of longitudinal and transverse waves at 10 MH_{z} over the temperature range 3.0 to 11^{o} K are given.

17. Key Words (Suggested by Author(s))	18. Distribution Statement
Ultrasonic attenuation Superconductors Niobium	Unclassified - unlimited

19. Security Classif. (of this report)	20. Security Classif. (of this page)	21. No. of Pages	22. Price*
Unclassified	Unclassified	84	$3.00

*For sale by the National Technical Information Service, Springfield, Virginia 22151

FOREWORD

The work described in this report was conducted at John Carroll University under NASA grant NGR 36-006-003 with James C. Laurence of the Lewis Research Center Electromagnetic Propulsion Division as the NASA Project Manager.

TABLE OF CONTENTS

I INTRODUCTION

Many investigators have studied the dependence of the ultrasonic attenuation and the elastic moduli of superconductors on temperature, external magnetic field, and ultrasonic frequency. Most of the studies reported have employed longitudinal waves. For weak coupling superconductors, the dependence of the ultrasonic attenuation of longitudinal waves on temperature was found to agree with the Bardeen, Cooper, and Schrieffer[1] (BCS) theory of superconductivity. This agreement was independent of the $q\ell$ value where q is the sound wave number and ℓ is the electron mean free path. The energy gap determined from this data was in substantial agreement with the BCS theory. However, anomalous behavior of the ultrasonic attenuation as a function of temperature has been reported in strong coupling superconductors and also in niobium which is an intermediate coupling superconductor. In the case of transverse waves for $q\ell<1$, the attenuation follows the BCS prediction. For $q\ell>1$ a rapid fall of the attenuation due to a shorting out of the Meissner effect has been observed. The rapid fall is followed by a more gradual curve which agrees with the BCS prediction[2].

For type II superconductors, extensive measurements of the magnetic field dependence of the attenuation in the mixed state have

also been reported. These studies have principally employed longitudinal waves. Rudnick et al.[3], Gottlieb et al.[4], and Ikushima et al.[5] have investigated the mixed state of niobium using longitudinal waves. Their results have been in qualitative agreement with the Maki[6,7] theory of ultrasonic attenuation in the mixed state. The only results for transverse waves in niobium have been by Rudnick et al. for one frequency and by Slotwinski[8] for the ultrasonic propagation direction perpendicular to the magnetic field.

The present study was undertaken to investigate the temperature dependence of the ultrasonic attenuation for longitudinal and transverse waves in niobium. Deviations from the BCS theory was investigated over a large spectrum of frequencies and sample purities. Included in this study is an examination of the magnetic field dependence of the attenuation of shear waves in the mixed state near the upper critical field.

Concurrent with this investigation, the behavior of the elastic moduli at the superconducting transition was studied. This portion of the study was undertaken to accurately determine the variation in the elastic moduli in the normal and superconducting states of a type II superconductor.

II THEORY

Temperature Dependence of the Ultrasonic Attenuation

Early investigations indicated that the ultrasonic attenuation decreased rapidly with temperature below the critical temperature T_c. This was believed to be caused by the rapid decrease in the population density of the normal electrons. Following this suposition, the BCS[1] theory of superconductivity predicts the temperature dependence of the ultrasonic attenuation for longitudinal waves in isotropic, weak coupling superconductors to be

$$\frac{\alpha_s}{\alpha_n} = 2F(\Delta) = \frac{2}{1 + e^{\Delta(T)/kT}} \qquad (1)$$

where α_s and α_n are the ultrasonic wave attenuations in the superconducting and normal states respectively, and $F(\Delta)$ is the Fermi distribution function of the temperature dependent energy gap $\Delta(T)$. This relation was derived for the case where the phonon energy is very small compared with the 0°K energy gap $\Delta(0)$ and for the limit $q\ell >> 1$. Tsuneto[9] later showed that this equation is valid for arbitrary $q\ell$ as long as the mean free path is impurity limited.

Equation 1 was derived for longitudinal waves, but the shear wave attenuation in some metals has been shown to also have the BCS temperature dependence for $q\ell << 1$. However, studies by Morse et al.[10]

in tin and by Claiborne and Morse[11] in aluminum showed that the attenuation does not follow BCS when $q\ell>1$ but instead drops rapidly just below the transition temperature and then falls more gradually. The fraction of the total attenuation attributed to this rapid fall attenuation was reported[11] to be a function of $q\ell$. Although the attenuation decreased rapidly over a very narrow region of temperature, it was not considered discontinuous. Claiborne and Morse approached this problem by dividing the ultrasonic attenuation into two temperature regions: a rapid fall region near T_c, and a residual region which obeys the BCS temperature dependence. The attenuation in the superconducting state $\alpha_s(T)$ is written as $\alpha_r(T)$ below T_c, and as $\alpha_r(T_c) + \alpha_E$ at T_c. α_E is the amount of rapid fall attenuation just below T_c, and $\alpha_r(T)$ is the amount of attenuation remaining at temperature T. The rapid fall region is assumed to result from an electromagnetic interaction in which the superconducting electrons are screened by the ionic cores. This interaction is a function of $q\ell$; as $q\ell$ becomes larger the ratio $\alpha_E/\alpha_n(T_c)$ becomes larger. However for $q\ell<1$ the interaction becomes negligible. To take this interaction into account Equation 1 was modified to read

$$\frac{\alpha_r}{\alpha_n} = g2F(\Delta) \qquad (2)$$

g is the same parameter which appears in Pippard's[12] free electron attenuation expression for transverse waves. g is a function of $q\ell$ and varies from 1 for low $q\ell$ values to 0 for very large $q\ell$. Claiborne and Morse successfully applied this approach to their results for aluminum. It is important to note that they were limited to $q\ell$ values

between about .1 and 3.

Later studies in aluminum by David et al.[13] for higher values of $q\ell$ indicated that although the rapid fall attenuation was a function of $q\ell$, the functional form predicted by Claiborne and Morse did not agree with experimental data. Leibowitz[14] expanded the approach of Claiborne and Morse to include a deformation term to account for real metal effects not considered in the free electron approximation of Claiborne and Morse. In the Leibowitz formulation, g is replaced by two terms: a collision drag term and a deformation term. In the free electron limit, Leibowitz's approach reduces to the Claiborne and Morse treatment, and both models reduce to BCS for $q\ell<1$.

Regardless of the behavior of the attenuation of shear waves near T_c, the BCS expression was found to agree with experimental results at temperatures well below T_c. Therefore, the zero temperature energy gap $\Delta(0)$ can be determined; and the gaps determined are in excellent agreement with longitudinal wave measurements and energy gaps determined by other methods.

Magnetic Field Dependence of the Ultrasonic Attenuation

The BCS theory is unable to predict the behavior of the ultrasonic attenuation as a function of magnetic field in type II superconductors. Maki[6,7] proposed a mathematical model to explain the ultrasonic attenuation in the mixed state. This theory was

developed for the region near H_{c2} for $q\ell>1$. The behavior of the attenuation near H_{c2} is expected to be a function of the angle between the direction of the applied magnetic field and the direction of ultrasonic wave propagation. This is expected since the electrons associated with the fluxoids have a different order parameter perpendicular and parallel to them. This difference becomes important at frequencies above 100 MHz[4]. The Maki formalism was extended by Kinder for intermediate $q\ell$ values. The Maki-Kinder expressions are as follows:

$$1 - \frac{\alpha_s}{\alpha_n} = C_1(H_{c2}-H)^{1/2} \tag{3}$$

$$g(q\ell) - \frac{\alpha_s}{\alpha_n} = C_2(H_{c2}-H)^{1/2} \tag{4}$$

where the proportionality constants C_1 and C_2 are functions of temperature, $q\ell$, purity, and angle between the magnetic field direction and ultrasonic wave propagation. For large $q\ell$, the Pippard function $g(q\ell)$ must be included as shown by Eq. (4). The Maki-Kinder slopes, C_1 and C_2, can be determined directly from measurements of the attenuation ratio, α_s/α_n.

Ultrasonic methods are particularly useful here since ultrasonic waves penetrate into the bulk of the material; whereas, techniques involving electromagnetic waves penetrate only to the skin depth. The directionality of ultrasonic propagation can be used to study any anisotropies. Electromagnetic waves tend to average any anisotropies[4].

Magnetization techniques also provide a useful means of studying the bulk properties of superconductors. Figure 1 shows a

comparison of the magnetization and the ultrasonic attenuation in the mixed state, illustrating the greater sensitivity of the ultrasonic attenuation in the mixed state near the critical field. For this reason, ultrasonic attenuation measurements can provide accurate information on the details of the mixed state. An illustration of the value of ultrasonic measurements is the observed anisotropy of H_{c2} by Slotwinski[8]. Slotwinski's results are shown in Figure 2. The anisotropy was determined to be approximately 3 per cent of the value of H_{c2}.

III EXPERIMENTAL PROCEDURE

Sample Preparation

The acoustic specimens were cut from two different single crystal boules which were 7 mm. and 9 mm. in diameter. The samples were oriented within 0.2° of the [110] direction using the Laue backscattering method. For this orientation the three independent waves corresponsing to the elastic constants C_L, C_{44}, and C' can be studied. The samples were cut on a spark cutter and carefully hand lapped so that the faces were parallel to better than five microns. Sample A had a length of 1.73 mm. and a diameter of 7 mm. Sample C had a length of 11.4 mm. and a diameter of 7 mm. Sample B was 9.35 mm. long and 9 mm. in diameter. Sample D was also cut from the 9 mm. boule, but this time two parallel [100] faces were lapped. These faces were 5.30 mm. apart. Most of the high frequency attenuation data was taken using Sample A in order that the total range of the attenuation change would be within the dynamic range of the receiving system. The larger samples were used for the low frequency attenuation and velocity measurements.

The samples were treated by an oxidation annealing process. In this process, the samples were first heated for several hours in an oxygen atmosphere of 10^{-6} Torr to a temperature below the ignition temperature of carbon monoxide. The oxygen combined with

the carbon impurities in the niobium sample. The sample was then heated in a vacuum exceeding 10^{-9} Torr to within 100°C of the melting point of niobium. The carbon monoxide outgassed from the sample as did any oxygen, hydrogen, or nitrogen trapped in the sample. Visible outgassing ceased after six hours. However, the samples were heated for ten hours to insure maximum removal of impurities and then cooled to room temperature. The long heating period also relaxed strains in the crystal. The samples were not relapped so that new strains were not introduced. The samples were stored in liquid nitrogen to prohibit oxidation and to inhibit gases such as hydrogen from entering the sample.

The oxidation annealing process was found to increase the mean free path in Sample A by 2 and in Sample B by 4. To date, measurements were not made on Sample C after annealing. The residual resistance ratio was estimated to be about 400 in Sample A and 150 in Sample B.

An additional benefit of the annealing process was the elimination of the trapped flux effect. This occurs after the sample has been subjected to a magnetic field greater than the lower critical field. Flux is trapped in the sample by circulating currents through multiply connected regions. This is observed as a residual attenuation or hysteresis in the attenuation versus magnetic field plots. Before annealing, the trapped flux effect was observed to be about 10 per cent of the total attenuation change. After annealing, the trapped flux

effect was not observable as determined by the lack of hysteresis in the attenuation versus magnetic field plots.

Attenuation Measurements

The ultrasonic pulse echo technique was used to study the attenuation of ultrasonic waves. Attenuation measurements were made by observing the change in pulse amplitude of the acoustic pulse as a function of applied magnetic field, sample temperature, or ultrasonic frequency. A schematic diagram of the system used in attenuation measurements is shown in Figure 3. A Matec pulsed oscillator produced the acoustic pulses by exciting a quartz transducer of 10 MHz fundamental frequency. The acoustic signal was transmitted to the niobium sample through a thin layer of Dow Corning 200 fluid. After the acoustic wave had propagated through the sample, it was received by a similarly bonded transducer at the opposite face of the sample. The electrical signal from the receiving transducer was mixed in a LEL mixer-preamp with the signal from a Hewlett-Packard local oscillator which was adjusted to plus or minus 60 MHz of the Matec pulsed oscillator. An LEL 60 MHz i.f. strip amplified the signal completing the hetrodyne circuit. The detected signal, in the form of one to two microsecond wide pulses, was displayed on a Hewlett-Packard Model 175 A oscilloscope which produces a D.C. signal proportional to the height of any given echo. The D.C. output signal was then applied to a Brookdeal phase sensitive detector. The variation in the attenuation in dB was calibrated using a Hewlett-Packard

Model 606 D which contained a calibrated piston attenuator. This output was applied to the same electronics as the received acoustic pulse, thus compensating for any nonlinearities in the receiver amplifiers.

The system was controlled by a sequential gating logic circuit which provided trigger pulses to circuit components and a reference signal to the phase sensitive detector[15]. The system timing was arranged on two timing gates. On Gate A the Matec pulsed oscillator was triggered, and on Gate B the comparator pulse was triggered. The Hewlett-Packard oscilloscope was triggered on every gate. The system was arranged so that Gate A could occur several consecutive times then Gate B would occur the same number of times. This permitted the oscilloscope circuitry to charge to the value corresponding to each gate. For example, Gate A could occur twice, then Gate B would occur twice again, and so on. The logic system included an adjustable pulse delay circuit for positioning the comparator pulse at the desired echo and an adjustable pulse-delay circuit for blanking the local oscillator during the time the Matec pulsed-oscillator operated. This prevented overdriving the receiver. The system permitted relative attenuation calibration to better than 0.2 db.

Velocity Measurements

A continuous wave (cw) method was used in the study of ultrasonic velocity changes[16]. Measurements were taken by recording the change in frequency of the continuous-wave oscillator. This can

be related to the change in velocity as a function of magnetic field or temperature. A schematic diagram of the system used in velocity measurements is shown in Figure 4. The continuous-wave output of a Hewlett-Packard Model 608 F oscillator, stabilized by a Hewlett-Packard Model 8708 A synchronizer, was applied to a composite resonator of length L made up of a transmitting quartz transducer-niobium sample-receiving quartz transducer. Corresponding to this resonator, there existed a spectrum of mechanical resonances ω_n separated by $f = f_{n+1} - f_n = \frac{v}{2L}$ where v is the sound velocity, and quality factors are $Q = \omega_n/2\alpha$ where α is the acoustic attenuation in inverse seconds. Superimposed on the mechanical resonance spectrum was the frequency response of the quartz transducers.

An integral number of half-wave lengths of sound were necessary for the system to be in mechanical resonance, i.e., $L = n\frac{\lambda_o}{2}$ where $\lambda_o = \frac{v_o}{f_o}$. The zero subscripts indicate zero magnetic field or initial temperature. If a magnetic field was applied to the sample or the temperature of the sample was varied, the velocity of the acoustic wave was changed to $v = v_o + \delta v$, and the system was no longer in mechanical resonance. The frequency was changed to $f = f_o + \delta f$ to again achieve resonance. The above expressions result in $\delta v = \lambda_o \delta f$ or $\frac{\delta v}{v} = \frac{\delta f}{f}$. The change in velocity can, therefore, be measured by determining the change in frequency required to bring the system back to resonance.

The curve of received signal amplitude versus frequency for longitudinal waves in niobium at 77°K is shown in Figure 5. Each

mechanical resonance peak has a width given by the Q of the circuit at that frequency. Referring to Figure 5, if the rf oscillator frequency modulated by a 200 Hz audio signal was adjusted to some frequency slightly higher than ω_n, the received signal would be amplitude modulated at the 200 Hz frequency with an amplitude dependent on the slope of the resonance at ω.[17] The amplitude modulation would be 180° out of phase with the FM signal; that is, when the FM signal deviated to a higher rf frequency, the amplitude would decrease, and when the FM signal deviated to a lower rf frequency, the amplitude would increase. If ω were less than ω_n, the amplitude modulation would be in phase with the FM signal. If $\omega = \omega_n$, the rf carrier is modulated at some even multiple of 200 Hz. This argument assumes a continuum about ω_n. To achieve an approximation to this condition, a modulation index of approximately ten was used. This permitted several orders of side bands to lie within the rf frequency deviation.

In this system, the frequency modulated rf signal was adjusted to ω_n. The received amplitude and frequency modulated rf signal were amplitude modulation detected. The phase of the resulting audio signal was amplified and compared to the original phase shifted audio signal using a phase sensitive detector. The amplifier incorporated filters to reject all but the fundamental audio frequency. The original audio signal was phase shifted to be in phase (or 180° out of phase) with the detected fundamental audio signal. When the rf oscillator was adjusted to ω_n, the phase sensitive detector indicated zero deflection. This permitted precise location of the resonance peak. If the magnetic field or temperature was varied, the velocity

of sound in the sample would change, and the resonance peak would shift resulting in the rf carrier becoming amplitude modulated. An error signal proportional to the phase sensitive detector's output would indicate the direction of this resonance peak shift. The output of the phase sensitive detector through a correction amplifier provided a voltage to the Hewlett-Packard 608 F to change the frequency. This arrangement enabled the frequency to be adjusted to follow the resonance peak. A general Radio Model 1191 B frequency counter and a General Radio Model 1136 digital to analog converter provided a means of automatically recording the frequency changes as a function of magnetic field on a Mosely X-Y Chart recorder.

Magnet

The magnetic field was provided by a 12" Harvey Wells electromagnet. The power supply of the electromagnet was controlled by a magnet sweep generator which allowed the field to be swept linearly in time from 0 to 14 kilogauss in one half kilogauss increments. Sweep times of one kilogauss per minute were found acceptable. The magnet sweep generator provided a voltage from the Hall probe magnetic field detector for driving the X-axis of the X-Y chart recorder. A Rawson rotating coil gaussmeter accurate to .1 per cent was used for field calibration. The X-axis of the chart recorder was offset to achieve a resolution of 5 gauss per millimeter on the recorder for field values between H_{c1} and H_{c2}.

The niobium sample was cooled from the normal to the superconducting state in zero applied magnetic field. Since the magnet

had a residual magnetic field of approximately 30 gauss, coils were attached to the poles to permit variable cancellation of fields of plus or minus 40 gauss. The lowest range on the gaussmeter was the 100 gauss scale. The residual field could be adjusted to zero gauss within one gauss.

Sample Holder

The design of the sample holder was found to be critical for the velocity and temperature measurements. The sample holder was of the same design as others previously used in this laboratory.

In order to have meaningful temperature measurements, it was necessary to have the sample and thermometer in good thermal contact. To accomplish this, the sample was thermally anchored to the bottom block of the sample holder by a .25" wide and .010" thick copper strap. The strap was tightly fastened by a spring loaded arrangement about the sample or about the quartz delay rod for Sample A. The other end of the strap was securely bolted to the bottom plate. The bottom section of the sample holder was made of an aluminum alloy selected for good thermal conductivity at liquid helium temperature. The thermometers were located less than .2" from the sample. The thermometers were mounted using GE heat varnish in the bottom section around which the heater was wound noninductively using Evan-ohm resistance wire. The close proximity of the temperature controller thermometer to the heater reduced the delay time between heat input and temperature change.

This reduced the possibility of the temperature control system thermally oscillating.

Prevention of interelectrode electromagnetic coupling within the sample holder was found necessary for meaningful velocity measurements. Since a continuous-wave signal was used, the receiver and transmitter leads were electrically isolated in order to reduce leakage. If a leakage signal was present, the total received signal would be a vector sum (using a phasor description) of the electrical signal converted from acoustic waves plus the leakage signal at some angle with respect to the acoustic-electric signal. If the temperature of the sample or the external field were changed, the strength of the received signal would change (the length of the phasor would change). Since the total received signal depends on the magnitude and angle of the components, the leakage signal can result in false values for the magnitude of the velocity change. Incorrect directions of change can result if the leakage signal is large enough. A complete mathematical analysis of the problem of leakage is described in the Appendix.

The sample holder was, therefore, modified to reduce leakage. The transducer contact buttons were depressed flush with the sample holder surface. The sample was grounded by a copper strap. In addition, copper washers were placed around the outside edge of the transducers such that they were in contact with the sample and the sample holder (the transducer's diameter was less than the inside diameter of the copper washer). The copper washers were wired to

electrical ground. Indium O-rings were soldered to both flat surfaces of each copper washer. The indium was pressed flat between the washer and the sample holder surface when the sample holder was assembled. The transmitter, receiver transducers, and contact buttons were thereby isolated. The result of the above technique was that the electrical signal measured between resonant peaks was less than 2 per cent of the signal on the resonant peak at 10 and 30 MHz. Before these precautions were observed, the ratio was 10 per cent to 30 per cent.

Temperature Control

The low temperatures and accurate temperature control required for this experiment were obtained by the controlled evaporation of liquid helium and heating the sample. The sample holder was placed in an Andonian stainless steel dewar. Helium gas was throttled over the sample thereby using the heat capacity of the gas and the latent heat of vaporization of the helium to cool the sample. The sample zone of the dewar was isolated from the helium reservoir. The pressure in the sample zone could be varied from 760 mm. to 30 microns using a Duo-Seal rotary vacuum pump. The throttling rate and pumping rate determined the base temperature of the sample which could be varied from about 1.8°K to room temperature.

The temperature could be varied above the base temperature by applying heat to the sample using a Cryogenics Research TC-101 temperature controller. A Germanium resistance thermometer supplied by Cryocal, Inc. was used as one side of a bridge circuit in the

temperature controller. The reference side of the bridge was a calibrated variable resistor. The error signal from the bridge controlled a servo motor which controlled the current supplied to a heater on the sample holder. By adjusting the reference resistor the amount of heater current could be changed thereby changing the temperature of the sample.

The Germanium resistance thermometer used in the temperature controller was calibrated using a four-terminal resistance technique against a standard Germanium thermometer supplied by Andonian associates. Both thermometers were cooled to low temperatures, and the reference resistor setting of the temperature controller versus the temperature was recorded using the standard thermometer to determine the temperature. A computer program of a power series expansion of temperature as a function of resistance provided a tabulation of temperature versus temperature controller setting.

The temperature of the sample was determined using a second Germanium resistance thermometer independent of the temperature controller. This thermometer was calibrated between 1.5°K and 20°K by the manufacturer, Cryocal, Inc. The temperature controller thermometer had a resistance of approximately 250 ohms at 4.2°K while the resistance of the second thermometer was approximately 1,000 ohms at 4.2°K. Since the power dissipated in the thermometer was limited to a microwatt, the current through the thermometer was limited to 10 microamps at 4.2°K and 20 microamps near the

transition temperature of niobium. The higher resistance thermometer provided a more accurate determination of the temperature near the transition temperature. The lower resistance thermometer was better suited to the temperature controller operation in the region 2°K to 10°K. This resistor permitted control of temperature over this range using a single scale on the temperature controller. In order to determine the temperature of the sample, the resistance of the second thermometer was measured using a constant current source supplied by Keithley Instrument Corp. and a Data Technology digital voltmeter. The temperature was determined from a calibration table. The constant current source was stable to .02 per cent of the reading, and the digital voltmeter permitted readings accurate to plus or minus two microvolts. Since the sample was in good thermal contact with the thermometers, the temperature of the sample was known to plus or minus 20 millidegrees.

Using the second thermometer it was found that the temperature controller maintained temperatures well within 20 millidegrees. The variable resistor in the temperature controller consisted of a course selector switch and a ten-turn potentiometer. If the temperature was changed using the course switch and the ten-turn potentiometer setting was not disturbed, the temperature was reproducible within 20 millidegrees. Backlash in the ten-turn potentiometer reduced reproducability to 100 millidegrees when this control was changed.

IV RESULTS AND DISCUSSION

Temperature Dependence of the Attenuation

A typical plot of the ultrasonic attenuation as a function of temperature is shown in Figure 6. Below the critical temperature, T_c, the attenuation in the normal state rises slightly reaching a constant value, $\alpha_n(0)$. The normal curve was obtained by applying a magnetic field greater than that required to destroy superconductivity. For high purity crystals, $\alpha_n(0)$ is a function of magnetic field due to the magnetoacoustic effect. In this study $\alpha_n(0)$ changed only for fields much greater than those required to make niobium normal. The attenuation in the superconducting state falls rapidly and approaches a constant value α_{so} for $T<T_c/4$. α_{so} represents the attenuation caused by mechanisms other than interactions with electrons. Therefore, the difference between a measured α and α_{so} represents the contribution due to the conduction electrons.

A study of α_n for $T<T_c/4$ as a function of frequency can be used to compare relative sample purities. The attenuation due to electrons in a normal metal is proportional to frequency squared and the electron mean free path in the region $q\ell<<1$. For $q\ell>>1$ the attenuation changes to a linear dependence on frequency and is

independent of the electron mean free path. Figures 7, 8, and 9 show log α_n versus log f for longitudinal waves and for two transverse waves corresponding to C' and C_{44}. All waves were propagated in the [110] direction. For low frequencies the frequency squared dependence of the attenuation is clearly seen.

Since the attenuation depends on $q^2\ell$ in the region $q\ell<<1$, for a given propagation direction, mode, and frequency the ratio of α_n for two samples provides the ratio of the electron mean free paths. Figure 10 is a plot of log α_n versus log f for Sample A and for a sample used by Perz and Dobbs[18]. Direct comparison indicates that Sample A is approximately 30 per cent better than that used by Perz and Dobbs. Sample B was determined to be about one third as good as Sample A. The residual resistance ratio of the sample used by Perz and Dobbs was estimated to be 300. Thus, the ratio for Sample A would be about 400, and for Sample B it would be about 150.

Figure 11 is a plot of α_n versus f^2 for longitudinal waves in Sample A. This clearly shows that the attenuation departs from a frequency squared dependence above 500 MHz. This frequency corresponds to $q\ell$ values of the order of 1 and an electron mean free path length of approximately 0.002 mm. Referring to Figures 8 and 9, the attenuation of the transverse modes departs from a frequency squared dependence at approximately 270 MHz and 170 MHz for C' and C_{44}. This frequency also corresponds to a $q\ell$ value of the order of 1 because the q value of the shear wave is higher for a given frequency.

Typical plots of the reduced ultrasonic attenuation of longitudinal waves versus reduced temperature are shown in Figure 12. The plots are for Sample A at a high frequency and Sample B at a low frequency providing a wide range of $q\ell$ values. Both curves display a rapid fall immediately below T_c when compared with the BCS curve. For larger $q\ell$, the deviation from the BCS curve appears to be greater.

A typical plot of reduced attenuation versus temperature is shown in Figure 13 for the propagation mode corresponding to C'. The reduced attenuation of a wave corresponding to C_{44} behaves similarly and is shown in Figure 14. For all frequencies note the rapid fall region followed by a more gradual decrease in the attenuation.

For both longitudinal and transverse waves, the ultrasonic attenuation as a function of temperature agrees with BCS sufficiently well at temperatures much less than T_c to obtain an energy gap. As suggested by Perz,[19] Equation 1 for the ultrasonic attenuation as a function of temperature can be rearranged to the form

$$[\ell n(\frac{2\alpha_n}{\alpha_s} - 1)]^{-1} = \frac{At}{\Delta^*} \qquad (5)$$

where $t = T/T_c$, the reduced temperature, and $\Delta^* = \Delta(T)/\Delta(0)$, the reduced energy gap parameter. The temperature dependence of the energy gap was assumed to follow the BCS theory at low temperatures. A is related to the value of the 0°K energy gap by

$$\frac{A}{2} = \frac{\Delta(0)}{kT_c} \qquad (6)$$

A typical plot of $[\ell n(\frac{2\alpha_n}{\alpha_s} - 1)]^{-1}$ versus t/Δ^* is shown in Figure 15 for transverse waves. When plotted in this manner the curve should pass through the origin. The points near the origin are very sensitive to the value chosen for α_{so}, and α_{so} may be adjusted a few tenths of a dB for a best fit. The slope of these lines at low temperatures is A. The energy gaps for various directions were found to be within experimental error and independent of the mode in agreement with those reported by Perz and Dobbs[18] for longitudinal waves. Note that the curve is linear to about .7 T_c.

As shown in Figure 15, the curves may be linearized to .9 T_c if α_n is reduced by a certain amount of rapid fall attenuation and if the value of α_n is set equal to a constant given by $\alpha_n(T_c)$ minus the rapid fall attenuation at T_c. The resulting fit to BCS is shown in Figure 16. This method of analyzing the data is similar to the approach used in Al by Claiborne and Morse.[11] As mentioned before, this rapid fall attenuation is related to an electromagnetic interaction which should only be present for transverse waves with $q\ell>1$. Both our transverse and longitudinal wave attenuations could be fit to the BCS expression using this type of analysis even though $q\ell$ was not greater than one for the transverse case. The theory should not even apply for the longitudinal case. The results of this type of analysis for our data is presented in Table I. As will be discussed later, a more applicable method has been developed to explain the observed deviations of the attenuation from the BCS theory.

TABLE I
SUMMARY OF ATTENUATION DATA

Mode	Freq. (MHz)	$\frac{\Delta(0)}{k\ T_c}$	Rapid Fall Attenuation	$\alpha_{n_{dB}}(T_c)$	Rapid Fall Atten./$\alpha_n(T_c)$	Sample	T_c(°K)
C_L	150	1.77	2 dB	15.0	.13	B	9.50
C_L	450	1.84	3 dB	14.2	.21	A	9.20
C'	70	1.85	3 dB	19.7	.15	B	9.34
C'	90	1.79	2 dB	12.7	.16	B	9.26
C'	210	1.85	2 dB	11.5	.17	A	9.30
C'	290	1.89	2 dB	17.5	.11	A	9.26
C'	330	2.00	4 dB	22.0	.18	A	9.33
C'	410	1.89	6 dB	38.2	.16	A	9.22
C_{44}	50	1.77	1.3 dB	15.6	.08	B	9.26
C_{44}	92	1.89	0.8 dB	7.7	.10	A	9.30
C_{44}	153	1.89	3.0 dB	18.8	.16	A	9.33
C_{44}	212	1.90	4.0 dB	31.2	.13	A	9.33

As pointed out earlier, the BCS theory is valid in the case of longitudinal waves for $q\ell >> 1$. In this region, the attenuation in the normal state is independent of the mean free path. Since the attenuation in the superconducting state is given by $\alpha_s = 2F\alpha_n$, α_s simply exhibits the temperature dependence of the Fermi-Dirac distribution function, $F(\Delta)$. Tsuento[9] has extended the BCS theory to arbitrary $q\ell$ values but assumes that the mean free path is impurity limited. For this case then, α_n is again temperature independent regardless of the $q\ell$ value. In our studies a substantial temperature dependence of the normal state attenuation was observed for Sample A, (Figure 16) and a smaller temperature dependence was observed for Sample B (Figure 6). This indicates that in both samples the mean free path is phonon limited near T_c and becomes impurity limited at approximately 4°K. This behavior of the normal state attenuation may be compared to results obtained by other investigators who have made attenuation measurements in niobium.

Weber[20] has reported that for measurements on his sample using longitudinal waves the attenuation was proportional to the frequency squared below 130 MHz. At 30 MHz, the normal state attenuation exhibited a large temperature dependence and the attenuation in the superconducting state fell much faster than BCS. However, at 220 MHz with $q\ell > 1$, the normal state attenuation was independent of temperature and the attenuation in the superconducting state closely followed BCS behavior.

The measurements of Tsuda and Suzuki[21] on a sample of RR 830 also at 30 MHz showed a large temperature dependence in the normal state and a more rapid fall off than BCS in the superconducting state. Their data on this sample is shown in Figure 12. For their impure sample, the attenuation was found to follow BCS behavior. Based on the large value of H_{c2} listed for this sample compared with those obtained in the present study and the known dependence of H_{c2} on crystal purity,[22] it is believed that this crystal has a smaller mean free path than any employed in this study and therefore one expects the mean free path to be impurity limited. Thus the attenuation in the normal state is expected to be independent of temperature for arbitrary $q\ell$ values and the attenuation should and does follow BCS.

While the samples employed by Tsuda and Suzuki,[21] like our own, were carefully annealed, it is worthwhile pointing out that the direction of propagation in their samples deviated from the [110] by 4°. Kadanoff and Pippard[23] have recently pointed out that quasi-longitudinal waves which could be generated in this case, can exhibit a fall off faster than BCS. This, however, will not account for our own results nor the BCS behavior obtained by Tsuda and Suzuki on their impure crystal.

Perz and Dobbs[18] obtained results for a sample of comparable purity to Sample A at 290 MHz in agreement with our results for longitudinal waves. The normal state attenuation was temperature dependent and a rapid fall in the attenuation below T_c was obtained.

In any case, independent of the $q\ell$ value and the sample purity, the attenuation below $T_c/2$ does follow BCS and energy gaps of $1.8\ KT_c \pm .1$ were obtained.

Levy et al.[24] have studied the attenuation of shear waves in a very impure niobium crystal compared with Sample B. The attenuation in the normal state was temperature independent and the attenuation in the superconducting state followed BCS. They also obtained a value of the energy gap which is in agreement with the value obtained with longitudinal waves.

Our own studies with shear waves show effects which are similar to those obtained with longitudinal waves. For the range of $q\ell$ values employed, the attenuation in the normal state is temperature dependent as seen in Figure 16. The attenuation in the superconducting state always falls off faster than BCS. Since $q\ell$ has values estimated to be between 0.1 and 2 in this study, the function $g(q\ell)$ is essentially unity. Thus the formalism employed by Claiborne and Morse[11] to explain the rapid fall off in the shear wave attenuation of Al is not applicable. Because of the similarity in the behavior of both longitudinal and shear wave attenuations, and because of the low $q\ell$ values used, one cannot ascribe the rapid fall off near T_c to an electromagnetic interaction in which the superconducting electrons are screened by the ionic waves.

The results obtained in niobium are very similar to the effects observed by Fate, Shaw and Salinger[25] in lead. The important features to note are: (1) when the mean free path is phonon limited and $q\ell$

is less than one, α_s/α_n deviates from BCS behavior and exhibits a $q\ell$ dependence. The deviation is greater for larger $q\ell$ values. (2) When the mean free path is phonon-limited and $q\ell$ is much greater than one, α_s/α_n is independent of $q\ell$ and closely follows the BCS prediction. (3) When the mean free path is impurity limited over the entire temperature interval from T_c to 0 K, α_s/α_n is independent of $q\ell$ for all values of $q\ell$ and also follows the BCS behavior.

The data in Figure 16 clearly shows that the attenuation in the normal state is phonon limited to about 4 K where it becomes impurity limited. Since the effective mean free path at T_c is smaller than the impurity limited mean free path, the attenuation, which is a function of ℓ unless $q\ell>>1$, is less. By adding this temperature dependent difference to the normal state and to the superconducting state much closer agreement with BCS is obtained. This assumes that the phonon-limited mean free path and its temperature dependence is the same in both the superconducting and normal state.

Fate et al.[25] suggested that the phonon-limited mean free path is smaller in the superconducting state than in the normal state. This accounts for the $q\ell$ dependence observed when the mean free path is phonon-limited and would bring the corrected data discussed above in closer agreement with the BCS predictions since the correction must be larger for smaller mean free paths. Recently, Leibowitz et al.[26] have reported attenuation measurements of high frequency shear waves near T_c in an extremely pure niobium crystal. The attenuation ratio

was found to be frequency dependent and the deviation from BCS behavior was exactly opposite to what one would expect from the electromagnetic interaction formalism. That is, α_s at 30 MHz deviates substantially from BCS while the 270 MHz data, where he estimates $q\ell$ is 10, follows BCS more closely. For this $q\ell$ value, one expects the attenuation to be independent of mean free path while at 30 MHz the attenuation is still a function of ℓ which is phonon-limited. Thus Leibowitz's results are consistent with the mean free path formalism discussed above.

It should be pointed out that the rapid fall associated with the electromagnetic interaction should apply for $q\ell$ values much greater than one where the attenuation is independent of mean free path. Only than can a deviation from BCS behavior be associated with the electromagnetic interaction.

In summary the mean free path formalism accounts for the results obtained here and also explains the seemingly contradictory results previously obtained in niobium. It also accounts for the fact that despite the behavior of attenuations observed near T_c all investigators have obtained BCS behavior below $T_c/2$ where the mean free path is probably impurity limited for all samples. The values obtained for these energy gaps are in excellent agreement with those measured by other techniques.

While the phonon-limited mean free path mechanism explains semi-quantitatively all of the data, future studies over a wider range

of $q\ell$ values would be desirable to determine if quantitative agreement can be obtained.

Magnetic Field Dependence of the Attenuation

The magnetic field dependence of the ultrasonic attenuation is a function of temperature and ultrasonic frequency. In Figure 17, the relative attenuation is plotted against the reduced applied magnetic field, H/H_{c2}, for two temperatures and two frequencies. As indicated, the attenuation is a function of $q\ell$ in the mixed state.

H_{c2} is a function of the magnetic field direction relative to the propagation direction and crystallographic axis as discussed earlier. In this study H_{c2} was measured as 3235 gauss at 3.5°K for the magnetic field parallel to the [110] direction. This agrees with the data reported by Tsuda and Suzuki[21] for niobium having residual resistance ratios of 100 to 830.

The Kinder[27] formulation of the Maki theory predicts that the Maki slopes should be a function of the angle between the magnetic field and the ultrasonic propagation direction. The anisotropy in H_{c2} must be considered in determining the anisotropy in the slope. In this study, the ultrasonic wave was propagated along the [110] direction. The sample was positioned such that in one configuration the magnetic field was rotated always perpendicular to the propagation direction. In the other configuration, the magnetic field could be rotated to positions parallel and perpendicular to the propagation direction. This latter configuration was employed to study the

Kinder theory which predicts a difference in the Maki slopes for the magnetic field perpendicular and parallel to the propagation direction. For the $q\ell$ values used in this study, the Maki-Kinder expression for the relative attenuation as a function of magnetic field is

$$1 - \frac{\alpha_s}{\alpha_n} = C(H_{c2}-H)^{-1/2} \qquad (7)$$

where C is the Maki slope. In Figure 18, $1 - \frac{\alpha_s}{\alpha_n}$ vs. $(H_{c2}-H)^{1/2}$ is plotted for longitudinal waves for two different $q\ell$ values. The slope, C, is greater for the higher $q\ell$ value. Figures 19 and 20 are plots of $1 - \frac{\alpha_s}{\alpha_n}$ versus $(H_{c2}-H)^{1/2}$ for the two transverse modes corresponding to C' and C_{44}. Two $q\ell$ values are represented in each figure. The behavior of the slopes as a function of $q\ell$ is identical for both modes. Higher slopes were found for the larger $q\ell$ values.

The angular dependence of the Maki slopes is illustrated in Figures 21 and 22 where the plane of rotation is perpendicular to [001] direction and [110] direction respectively. All three modes are illustrated in Figure 21. In all cases, the direction of ultrasonic propagation is parallel to the [110] direction. For longitudinal waves, the slope is a minimum for H parallel to the $[1\bar{1}1]$ direction when H is rotated in the [110] plane. However, when H is rotated in the [001] plane, the slope is maximum when H is along the [100] plane. This illustrates that both the angle between H and q, along with the direction of H, determines the anisotropy in the slope. This may be related to the anisotropy observed in H_{c2} discussed earlier.[8] The slopes associated with the C' mode exhibit a similar behavior.

To compare the slope with theory,[27] we must use the data in Fig. 22. In this Figure H is along a [110] type direction when H is perpendicular or parallel to q. For transverse waves and low $q\ell$ values, the slopes are expected to be greater for H perpendicular to q than when H is parallel to q. The slope is also expected to peak where H is 45° from q. The C' data in Fig. 22 exhibits this behavior for a fixed value of $q\ell$. One should note, however, that for H perpendicular to q, the $q\ell$ dependence of the slope, which admittedly is small, is opposite to that of the Maki-Kinder theory.

For longitudinal waves, however, the theory predicts that for low $q\ell$ values, the anisotropy in the slopes should vary in a manner similar to the transverse case with the important exception that the slope reaches a minimum instead of a maximum value for an angle of 45° between q and H. This minimum predicted by the theory is clearly not observed as can be seen in Fig. 22. The $q\ell$ dependence on the slope for H perpendicular to q is again small but does agree with the theory.

Table II lists the Maki slopes as a function of temperature, ultrasonic frequency, mode, and orientation.

TABLE II
SUMMARY OF MAKI SLOPES

Mode	Sample	Temp. (°K)	Freq. (MHz)	Orientation		Slope $(\text{gauss})^{-1/2}$	H_{c2} (gauss)
				H ⊥ to	q		
C_L	A	3.5	510	$[1\bar{1}0]$	$q_\perp H$	.049	3270
C_L	A	3.5	510	[110]	$q_\parallel H$	.047	3277
C_L	B	3.5	70	$[1\bar{1}0]$	$q_\perp H$	.044	3190
C_L	B	3.5	70	$[1\bar{1}1]$	$q_\perp H$	.040	3166
C_L	B	3.5	70	[001]	$q_\perp H$	.041	3258
C'	A	5.5	290	$[1\bar{1}0]$	$q_\perp H$	.033	2280
C'	A	5.5	290	[110]	$q_\parallel H$	.028	2292
C'	A	3.5	290	$[1\bar{1}0]$	$q_\perp H$	.029	3135
C'	A	3.5	290	[110]	$q_\parallel H$	.027	3129
C'	B	3.5	150	$[1\bar{1}0]$	$q_\perp H$	.030	3363
C'	B	3.5	50	$[1\bar{1}0]$	$q_\perp H$	.031	3363
C'	B	3.5	50	$[1\bar{1}1]$	$q_\perp H$	.030	3451
C'	B	3.5	50	[001]	$q_\perp H$	.035	3209
C_{44}	B	3.5	90	[110]	$q_\perp H$	.040	3235
C_{44}	B	3.5	90	[111]	$q_\perp H$	.037	3278
C_{44}	B	3.5	90	[001]	$q_\perp H$	.044	3150
C_{44}	B	3.5	30	[110]	$q_\perp H$	.030	3243
C_{44}	B	3.5	30	[111]	$q_\perp H$	.033	3285
C_{44}	B	3.5	30	[001]	$q_\perp H$	.036	3171

Velocity of Ultrasonic Waves in the Normal and Superconducting States of Niobium

The only extensive measurements of the small variations of the ultrasonic velocity in niobium were made by Alers and Waldorf[28] using a modified "sing-around" technique. This technique, however, is extremely sensitive to attenuation changes which accompany the changes in velocity of the ultrasonic wave. In the present study, a continuous wave (cw) technique has been employed. Even though the sensitivity of this technique decreases when the attenuation of the ultrasonic wave increases, it is a more reliable method of measuring velocity changes than the technique used in the previous investigation.

From their study, Alers and Waldorf have reported the temperature dependence of the difference in the moduli between the normal and superconducting states of niobium. This difference is completely dominated by the variation of the velocity in the normal state. Little is therefore known about the temperature dependence of the moduli in the superconducting state.

It should also be noted that the crystals used in this study are purer than those used in the previous report. Since these crystals have been annealed, they show no trapped flux effects which may give rise to anomalous effects.

Since the time of Alers and Waldorf's study, Bernstein[29,30] has developed a theory of the electronic contribution to the temperature dependence of the elastic constants in the normal and superconducting states. The results of this investigation will be compared to his theory.

For these reasons, a systematic study of the changes in the velocity corresponding to the three independent elastic constants C_L, C_{44}, and C' was made in the normal and superconducting states of niobium.

In the normal state, the temperature dependence of the ultrasonic velocity, and hence the moduli, is dominated by two contributions to the free energy of the crystal: (1) the energy of the electron gas and (2) the lattice energy of the crystal. Since the elastic moduli are the second derivatives of the energy with respect to the strain they are expected to exhibit the same temperature dependence as the free energy.

The variation of the frequency and hence the velocity in both the normal and superconducting states is shown in Figures 23, 24, and 25 for the longitudinal and two transverse modes in Sample B. The fractional change in the elastic modulus is just twice the corresponding fractional change in the frequency. In table III, the fractional change in the velocity associated with the three elastic moduli at 3 K is listed along with the corresponding changes reported by Alers and Waldorf. It should be pointed out that our measurements were made on several resonance peaks and in several different experimental runs. The observed changes were always within 5% of each other. As discussed in the Appendix, leakage signals can lead to apparent velocity shifts which are opposite in sign on alternate resonance peaks. Our data, however, is felt to have negligible shifts due to leakage at 10 MHz because of its reproducibility from run to run.

Table III

Summary of fractional velocity changes in Nb in Sample B

Mode	Temperature	Frequency	$\frac{\Delta f}{f}$ (ppm)	$\frac{\Delta f}{f}$ (Alers and Waldorf[28])
C_L	3.0 K	10 MHz	21.2 ± .5	12
C_L	3.0 K	30 MHz	18.8 ± .5	Not reported
C'	3.0 K	10 MHz	26.0 ± .5	9
C_{44}	3.0 K	10 MHz	121 ± 2	65

Discontinuity in the bulk modulus $(\frac{\Delta B}{B})$ at $T = T_c$	
Alers and Waldorf[28]	$.7 \times 10^{-6}$
Present Study	1.2×10^{-6}
Theoretical Prediction (Ref. 24)	$2.8 \times 10^{-6} - 7.8 \times 10^{-6}$

The changes in the velocity between the normal and superconducting states were also measured on a second single crystal (Sample C) which had a mean free path estimated to be three times larger than that of Sample B. The observed changes were found to be in agreement with the data reported for Sample B in Table III. Velocity measurements were also made at 30 MHz and the observed changes were substantially the same as that observed at 10 MHz. Since the attenuation is nine times larger at 30 MHz and therefore the leakage signal should also be larger, the 30 MHz data is not as accurate as that obtained at 10 MHz. Nevertheless, the observed changes appear to be independent of the ultrasonic frequency and electron mean free paths used in this study.

As seen in Table III, the changes of the velocity in this investigation are nearly twice those obtained by Alers and Waldorf. This discrepancy is probably associated with the accuracy of the techniques employed.

In Figure 26, the variation of the frequency in the vicinity of T_c for longitudinal waves is shown. A discontinuity at T_c appears to be present. The magnitude of this discontinuity is about 0.4 ppm which corresponds to a discontinuity in the bulk modulus of 1.2 ppm. While one expects a discontinuity in the longitudinal velocity at T_c because of the second order phase change associated with the normal to superconducting transition, the magnitude of the discontinuity, while larger than that observed by Alers, is still a factor of two smaller than one would expect from the relation

$$\Delta B/B = 4\pi B(\partial H_c/\partial P)_T^2 \qquad (8)$$

This expression has been evaluated and listed in Table III using the values for the variation of critical field with pressure listed by Gardner and Smith.[31] It is quite possible that this discrepancy is a function of sample purity since the critical field is known to be very sensitive to impurities.[22] Considering the small magnitude of the discontinuity and the temperature control needed to accurately determine the discontinuity the agreement with the thermodynamic relationship above is considered satisfactory.

The measurements in the normal state shown in Figures 23, 24, and 25 were made in a magnetic field of about 4 kilogauss for temperatures below $T_c/2$. Between $T_c/2$ and T_c, the strength of the magnetic field was decreased somewhat but still was greater than H_{c2} for that particular temperature. No substantial variation of the velocity with magnetic field was observed in this temperature region. At the lower temperatures and larger fields, however, a small dependence of the velocity with magnetic field was detected.

As mentioned earlier, the temperature dependence of the moduli is expected to be the same as the free energy. In the normal state, the energy of the electron gas is proportional to T^2 and the energy of the lattice in the Debye region is proportional to T^4. Therefore, one can write

$$C = C_o(1 - \alpha T^2 - \beta T^4) \qquad (9)$$

where C_o is the value of the modulus in the normal state at T = 0 and α and β are coefficients related to the electron and phonon terms respectively. While data was obtained for all three modes, the most extensive measurements were made for C_{44} since the largest changes were observed for this mode.

In Figure 27, the frequency changes in the normal state relative to T = 0 K are plotted for the C_{44} mode versus temperature for Sample B. The dotted curve is what one obtains if only the T^2 term were present. In Table IV, the values of α and β obtained from the normal state measurements are shown for each of the three moduli. The corresponding values determined by Alers and Waldorf are listed for comparison. It will be noted that in Figure 25 for the C_{44} mode, the phonon term has been subtracted off by using the data in Table IV so that the variation of the velocity attributable only to the electrons has been obtained. It has been assumed that the phonon term is the same in the normal and superconducting states. The temperature dependence of the difference in the moduli, or equivalently the velocity, between the superconducting and normal states can be seen to be dominated by the normal state changes for temperatures below 1/2 T_c. That is, below 1/2 T_c the difference in the velocity is also proportional to T^2. This is consistent with the predictions of Bernstein and also with the data of Alers and Waldorf. For this mode large enough changes were observed in the superconducting state to study the temperature dependence of the velocity. The actual data for the superconducting state is presented in Table V.

Table IV

Coefficients* α and β

Sample	Mode	α	β	α (Alers)
B	C_L	2.8×10^{-7}	1.0×10^{-9}	2.7×10^{-7}
C	C_L	2.8×10^{-7}	1.4×10^{-9}	
B	C'	1.8×10^{-7}	3.02×10^{-9}	2.3×10^{-7}
B	C_{44}	20×10^{-7}	2.12×10^{-9}	12.8×10^{-7}

*All numbers are known to within 10%

Table V

Tabulation of Superconducting velocity data for C_{44} mode in Sample B. (T_c = 9.415 K)

Temperature (°K)	Frequency (Hz)
2.00 ± .02 K	10,070,247 ± 5 Hz
4.16	270
4.37	276
4.80	290
4.88	294
5.11	303
5.52	322
6.04	348
6.50	374
7.00	409
7.50	444
8.00	482
8.51	523
9.00	566
9.235 ± .005 K	589
9.26	591
9.28	594
9.31	597
9.33	600
9.41	611

By analogy with the normal state, one expects that the velocity in the superconducting state should have the same temperature dependence as the free energy in the superconducting state. Unfortunately no simple expression for the free energy exists except near T = 0 K. Furthermore, Bernstein is concerned only with the temperature dependence of the difference in the moduli in the normal and superconducting state and in particular for temperatures below 1/2 T_c. The temperature dependence of the free energy is however given in tabular form by Muhlschlegel.[32] This temperature dependence is shown by the dotted line in Figure 28. It can be seen that for $T_c/T > 1.5$ ($t < .7$), the data is quite linear. This indicates that the dominant temperature dependent term in the free energy is an exponential. Near T = 0, Muhlschlegel gives the following expression for the free energy in the superconducting state:

$$F/C_n T_c = 0.89\ t^{1/2}\ e^{-1.76kT_c/T} - 0.2364. \qquad (10)$$

In this expression F is the free energy and C_n is the specific heat in the normal state. This equation is clearly not valid for $t > .4$ since the energy gap is temperature dependent for $t > .4$ and goes to zero at T_c. The variation of the ultrasonic velocity in the superconducting state using the data shown in Table V, corrected for the phonon contribution as shown in Figure 25, is also plotted in Figure 28. It can be seen that the temperature dependence closely follows the free energy temperature dependence. The slope of the two lines agree with one another to within 10%. It should be noted that the experimental slope is quite sensitive to errors in f_{so}, the frequency in the superconducting

state at T = 0 K. Since the slope of the theoretical curve may be sensitive to truncation errors in the tabulated data, the velocity of C_{44} waves is therefore considered to have the same temperature dependence within experimental error as the free energy in the superconducting state.

Because the free energy has a complicated temperature dependence over the entire temperature region below T_c, it is difficult to withdraw an energy gap from the data. This is analagous to the variation of the specific heat in the superconducting state which can not be related to $e^{-\Delta/kT}$ over the entire temperature range. Since the C_{44} velocity data does, however, closely follow the BCS free energy, one can assume that the zero temperature energy gap, if it can be extracted from the experimental data, must be close to a BCS value of 1.76 kT_c. This would be in agreement with the values obtained directly by attenuation measurements and from other methods in niobium.

As pointed out previously, the temperature dependence of the difference of the moduli is in agreement with the theory of Bernstein. The magnitude of the observed changes are however larger than his calculated values. For the two shear moduli at 3 K the experimental value of ΔC_{44} and $\Delta C'$ in units of 10^7 dynes/cm^2 are 7.50 and 3.25. The corresponding values listed by Bernstein are 4.84 and 2.42. Since the theory derives the change in terms of derivatives of the energy gap as a function of strain expressed in terms of the density of states, a detailed comparison to it requires a knowledge of the

Fermi surface of niobium which at the present time is not well known. It is clear, however, that the calculated changes are the correct order of magnitude and exhibit the correct temperature dependence. The velocity measurements therefore can be useful in providing information about the Fermi surface.

Some measurements of the velocity were also made in the mixed state. As an indication of the sensitivity of this technique, the values of H_{c_2} and the anisotropy in H_{c_2} obtained from these measurements are in excellent agreement with the corresponding results obtained from the attenuation measurements.

The cw technique employed to measure the velocity changes can also be used to measure small attenuation changes. The width of the resonance lines can be related to the attenuation present. To determine the magnitude of the attenuation, the linewidth of the resonance peaks must be measured. A complete development of the dependence of the strength of the resonance line as a function of frequency and attenuation both in the absence and presence of a leakage signal is given in the Appendix. In the absence of leakage, the output voltage is shown to be

$$|E_R|^2 = \frac{E_o^2}{2(\cosh 2\alpha L - \cos 2 q\ell)}. \qquad \text{(A-8)}$$

The resonance peaks occur whenever $2 q\ell = n\pi$ so that at resonance E_R will be a maximum. The resonances are separated by a frequency f which is determined by the sample length and velocity. The above expression has been programed by Carome and Fritsch[33] to obtain directly a plot

of the attenuation versus $\frac{\Delta f_{1/2}}{f}$, where $\Delta f_{1/2}$ is the difference between the center frequency, f_o, and the frequency where the line has a value equal to 1/2 its maximum value. Thus if one measures E_R at the frequencies for which E_R is equal to 1/2 its maximum value, $\Delta f_{1/2}$ can be found and hence the attenuation can be determined.

The resonance lines in the superconducting and normal states at 4 K and 10 MHz are shown in Figures 29 and 30. In the superconducting state where $\alpha_s \simeq 0$, the line is quite sharp and $\Delta f_{1/2} \simeq 250$ Hz. For this sample f is 100 KHz. In the normal state $\Delta f_{1/2} \simeq 1100$ Hz. From the plot in Figure 3 of reference 33 a change in attenuation of 0.16 dB/cm is obtained at 10 MHz. This attenuation change agrees quite well with attenuation measurements made by the ultrasonic pulse echo technique at higher ultrasonic frequencies and extrapolated to 10 MHz. The advantage of the cw technique is the greater sensitivity and much more accurate determination of the ultrasonic frequency. This measurement also indicates the excellent internal consistency of the cw method and provides further evidence for the reliability in the analysis of the resonance technique used to obtain the velocity data.

In conclusion then, the temperature dependence of the velocity in both the normal and superconducting states of niobium has been determined. The changes measured are larger than previously reported and in addition the temperature dependence of the velocity in the superconducting state has been found to closely follow the temperature dependence of the free energy from the BCS theory.

These velocity measurements may also provide additional information about the phase transition at $T = T_c$ and should be useful in providing information about the Fermi surface and the strain dependence of critical field and critical temperature.

The attenuation measurements made with the cw technique also are quite useful for studying attenuation at low ultrasonic frequencies where the attenuation is small and can be a valuable technique for studying attenuation changes in superconducting alloys where small attenuation changes are expected to occur.

APPENDIX

The magnitude of velocity shifts as a result of a change in magnetic field or temperature has been observed to differ depending on the resonance peak; that is, the velocity shift observed on one resonance peak was found to differ from the velocity shift observed on an adjacent resonance peak. The difference in the velocity shifts was correlated to the amount of electrical leakage signal. If the leakage signal was large, the difference was found to be large; and occasionally the algebraic sign of the velocity shifts were opposite. If the leakage was small, the results from adjacent peaks were nearly identical.

Yee and Gavenda[16] have reported similar effects. They explain that this anomalous behavior is caused by an interaction between the electrical signal produced by the quartz transducer from the acoustic signals and the electrical leakage signal. The reason for the anomalous velocity results is that the amplitude and the velocity of the acoustic signal changes as a function of magnetic field or temperature. The output of the detector is a result of the phase and amplitude of the acoustic-electric signal and the leakage signal. Since the adjacent resonance peaks are a result of even and

odd number of half wave lengths, the acoustic-electric signal changes phase on adjacent peaks. Hence, different results are obtained on adjacent peaks.

Following Yee and Gavanda, the total received electrical signal is composed of an electrical leakage signal $E_c e^{i\phi}$ and the acoustic-electrical signal E_a where the phase angle refers to the transmitter signal. The acoustic-electrical signal may be expressed as:

$$E_a = E_o \sum_{m=0}^{\infty} [e^{(iq-\alpha)L}]^{2m+1} \tag{A-1}$$

where α is the energy attenuation coefficient and m is the number of round trips of the acoustic signal through the sample. E_a may be expressed as:

$$E_a = E_o e^{(iq-\alpha)L} \sum_{m=0}^{\infty} [e^{(i2q-2\alpha)L}]^m \tag{A-2}$$

The sum may be expressed as a geometric series so that E_a may be written:

$$E_a = E_o \frac{e^{(iq-\alpha)L}}{1-e^{(i2q-2\alpha)L}} \tag{A-3}$$

or

$$E_a = E_o \frac{e^{iqL}\, e^{-\alpha L}}{1-e^{-2\alpha L}(\cos 2qL + i \sin 2qL)}$$

$$|E_a| = \frac{E_o e^{-\alpha L}}{[(1-e^{-2\alpha L}\cos 2qL)^2 + e^{-4\alpha L}\sin^2 2qL]^{1/2}} \tag{A-4}$$

The total received electrical signal is:

$$E_R = E_c e^{i\phi} + E_a \tag{A-5}$$

The power delivered to the receiver is proportional to:

$$|E_R|^2 = |E_c e^{i\phi} + E_a|^2$$

$$|E_a|^2 = \frac{E_o^2}{2(\cosh 2\alpha L - \cos 2qL)} \tag{A-6}$$

So

$$|E_R|^2 = E_c^2 + \frac{E_o^2 + 2E_oE_c[e^{\alpha L}\cos(\phi - qL) - e^{-\alpha L}\cos(\phi + qL)]}{2(\cosh 2\alpha L - \cos 2qL)} \tag{A-7}$$

The above expression is exact. This differs slightly from Yee and Gavenda's expression which is believed to contain errors.

If $E_c = 0$,

$$|E_R|^2 = \frac{E_o^2}{2(\cosh 2\alpha L - \cos 2qL)} \tag{A-8}$$

Maxima occur at $qL = n\pi$ or $L = n\lambda/2$ as expected.

Consider an apparent shift in resonance, qL, caused by E_c.

Let $\delta = qL - n\pi$

So

$$\frac{|E_R|^2}{E_o^2} = \frac{E_c^2}{E_o^2} + \frac{1 \pm \frac{2E_c}{E_o}[e^{\alpha L}\cos(\phi - \delta) - e^{-\alpha L}\cos(\phi + \delta)]}{2(\cosh 2\alpha L - \cos 2\delta)} \tag{A-9}$$

where + corresponds to an even n and - corresponds to an odd n. The amplitude of the alternate resonances differ according to the magnitude of E_c. Note that when the frequency is adjusted to a value between resonances, the amount of coupling may be judged by:

$$\frac{|E_R|^2}{E_o^2} = \frac{E_c^2}{E_o^2} \tag{A-10}$$

To find the new apparent resonances, the above expression is maximized.

$$\frac{d}{d\delta}\left(\frac{|E_R|^2}{E_o^2}\right) = 0 \tag{A-11}$$

$$(\cosh 2\alpha L - \cos 2\delta)\left(\pm \frac{2E_c}{E_o}[e^{\alpha L}\sin(\phi-\delta)+e^{-\alpha L}\sin(\phi+\delta)]\right)$$

$$- \left[1 \pm \frac{2E_c}{E_o}[e^{\alpha L}\cos(\phi-\delta)-e^{-\alpha L}\cos(\phi+\delta)]\right] 2\sin 2\delta = 0 \tag{A-11}$$

Note that δ, the apparent shift, is a function of attenuation which is magnetic field and temperature dependent.

For $\phi = 0$ or π, $\delta = 0$ and (A-12)

$$\frac{|E_R|^2}{E_o^2} = \frac{E_c^2}{E_o^2} + \frac{1}{4\sinh^2\alpha L} \pm \frac{E_c}{E_o \sinh \alpha L} \tag{A-13}$$

Note that there is no phase shift, but the amplitude on adjacent peaks is different.

For $\phi = \pi/2$

$$\sin \delta = \mp \frac{1-[1+(16E_c^2/E_o^2)(\cosh^2\alpha L \sinh^2\alpha L)]^{1/2}}{(4E_c/E_o)\cosh \alpha L} \tag{A-14}$$

and

$$\frac{|E_R|^2}{E_o^2} = \frac{E_c^2}{E_o^2} + \frac{1+[1+(16E_c^2/E_o^2)(\cosh^2\alpha L \sinh^2\alpha L)]^{1/2}}{8\sinh^2\alpha L} \tag{A-15}$$

Note that the phase shift differs in sign on adjacent peaks, but the amplitude is constant regardless of the resonance peak. Phase angles between $-\pi/2$ and $\pi/2$ produce varying degrees of phase shift and amplitude differences between adjacent peaks.

The total change in velocity can be written as a real change dependent on magnetic field or temperature and an apparent change dependent on the magnitude and phase angle of the leakage signal.

$$\left(\frac{\Delta V}{V}\right)_T = \left(\frac{\Delta V}{V}\right)_R + \left(\frac{\Delta V}{V}\right)_A \tag{A-16}$$

The apparent change may be expressed as

$$\left(\frac{\Delta V}{V}\right)_A = \left(\frac{\Delta f}{f}\right)_A = \frac{\delta}{n\pi} \tag{A-17}$$

In order to eliminate anomalous effects due to apparent phase shifts, the magnitude of the leakage signal must be reduced or the phase angle adjusted to 0 or π. Since the latter is difficult to measure or achieve, precautions were taken to reduce the amplitude of the coupled signal to less than 2 per cent of the electrical signal on the resonance peak. In order to determine the real phase shift, data from adjacent peaks was averaged. It is interesting to note that,

within experimental tolerances, data from all odd n peaks was the same. Data from all even n peaks was the same though different from the data from odd n peaks.

REFERENCES

1. Bardeen, J., Cooper, L. N., and Schrieffer, J. R., Phys. Rev. 108, 1175 (1957).
2. Morse, R. W., "Ultrasonic Attenuation in Metals at Low Temperatures," Progress in Cryogenics, K. Mendelssohn ed., Heywood and Company Ltd., 251 (1959).
3. Rudnick, I., Kagiwada, R., Levy, M., Kagiwada, H., and Maki, K., Phys. Rev. Letters 18, 74 (1967).
4. Gottlieb, M., Jones, C.K., and Garbuny, M., Phys. Letters 25, 107 (1967).
5. Ikushima, A., Kajimura, K., Akao, F., Phys. Letters 25, 151 (1967).
6. Maki, K., Phys. Rev. 156, 433 (1967).
7. Maki, K., Phys. Rev. 156, 437 (1967).
8. Slotwinski, T., Master's Thesis, John Carroll University (1969).
9. Tsuneto, T., Phys. Rev. 121, 402 (1961).
10. Morse, R., and Bohm, H., Phys. Rev. 108, 1094 (1957).
11. Claiborne, L., and Morse, R., Phys. Rev. 136, 893 (1964).
12. Pippard, A., Phil. Mag. 46, 1104 (1955).
13. David, R., van der Laan, H., and Poulis, N., Physica 29, 357 (1963).
14. Leibowitz, J., Phys. Rev. 136, A22 (1964).
15. Leskovec, R., Hunter, J. and Davenport, J., Rev. Sci. Instr., (To be published).

16. Yee, B., and Gavenda, J., Phys. Rev. 175, 805 (1968).

17. Melcher, R., Bolef, D., and Merry, J., Rev. Sci. Instr. 39, 1618 (1968).

18. Perz, J., and Dobbs, E., Proc. Roy. Soc. 296, 113 (1966).

19. Perz, J., Can. J. Phys. 47, 438 (1969).

20. Weber, R., Phys. Rev. 133, A1487 (1964).

21. Tsuda, N., and Suzuki, T., J. Phys. Chem. Solids 28, 2487 (1967).

22. DeSorbo, W., Phys. Rev. 132, 107 (1963).

23. Kadanoff, L., and Pippard, A., Proc. Roy. Soc. A292, 299 (1966).

24. Levy, M., Kajiwada, R., and Rudnick, I., Phys. Rev. 132, 2039 (1963).

25. Fate, W. A., Shaw, R. W., and Salinger, G. L., Phys. Rev. 172, 413 (1968).

26. Leibowitz, J. R., Sebastian, R., and Alexander, E., Bull. Amer. Phys. Soc. 15, 655 (April 1970).

27. Kinder, H., Phys. Letters 26A, 319 (1968).

28. Alers, G., and Waldorf, D., IBM Jour. 89 (1962).

29. Bernstein, Phys. Rev. 132, 50 (1963).

30. Bernstein, Phys. Rev. 137, 1404A (1965).

31. Gardner, W. E., and Smith, T. F., Phys. Rev. 144, 233 (1966).

32. Muhlschlegel, B., Zeitschrift fur Physik 155, 313 (1959).

33. Carome, E. F., and Fritsch, K. P., to be presented at Fifth Symposium on Thermophysical Properties, Oct. 1970.

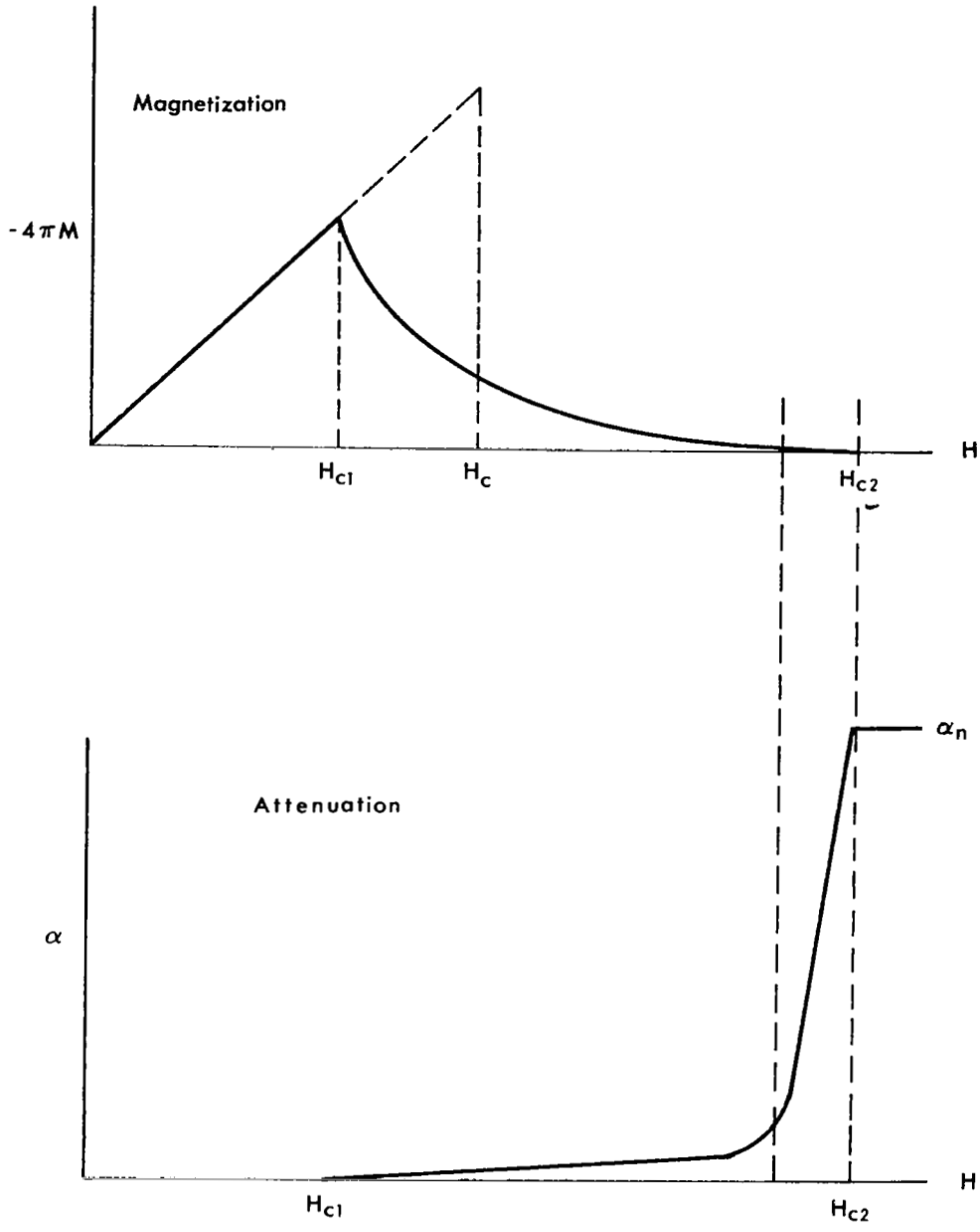

Figure 1. (a) Magnetization vs. applied magnetic field and (b) attenuation vs. applied magnetic field for a type II superconductor.

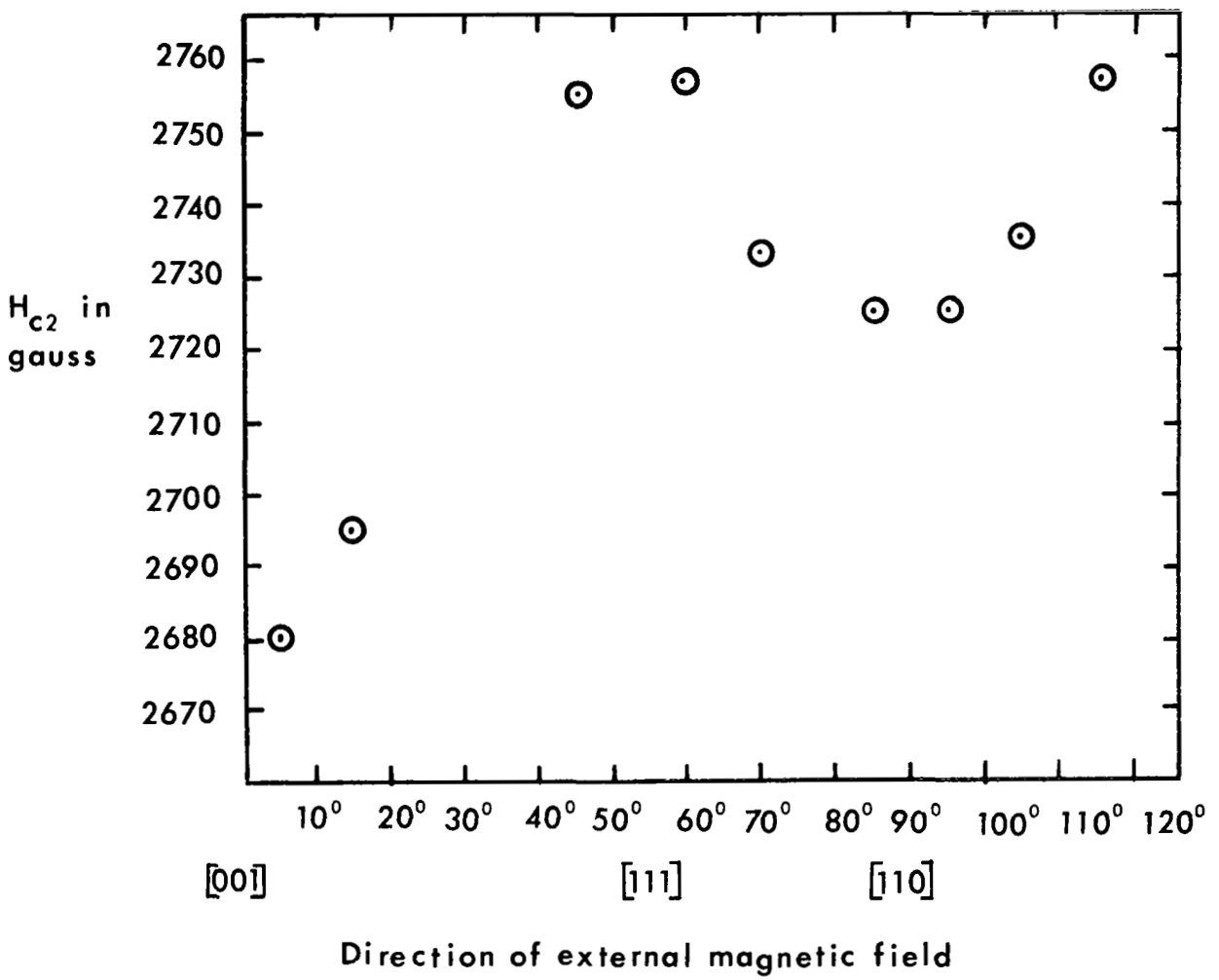

Figure 2. Anisotropy of H_{c2} as a function of the direction of applied magnetic field for shear wave propagation in [110] and polarized in $[1\bar{1}0]$ in Nb at 4.5°K. (Reproduced from a master's thesis (1969) by T. C. Slotwinski).

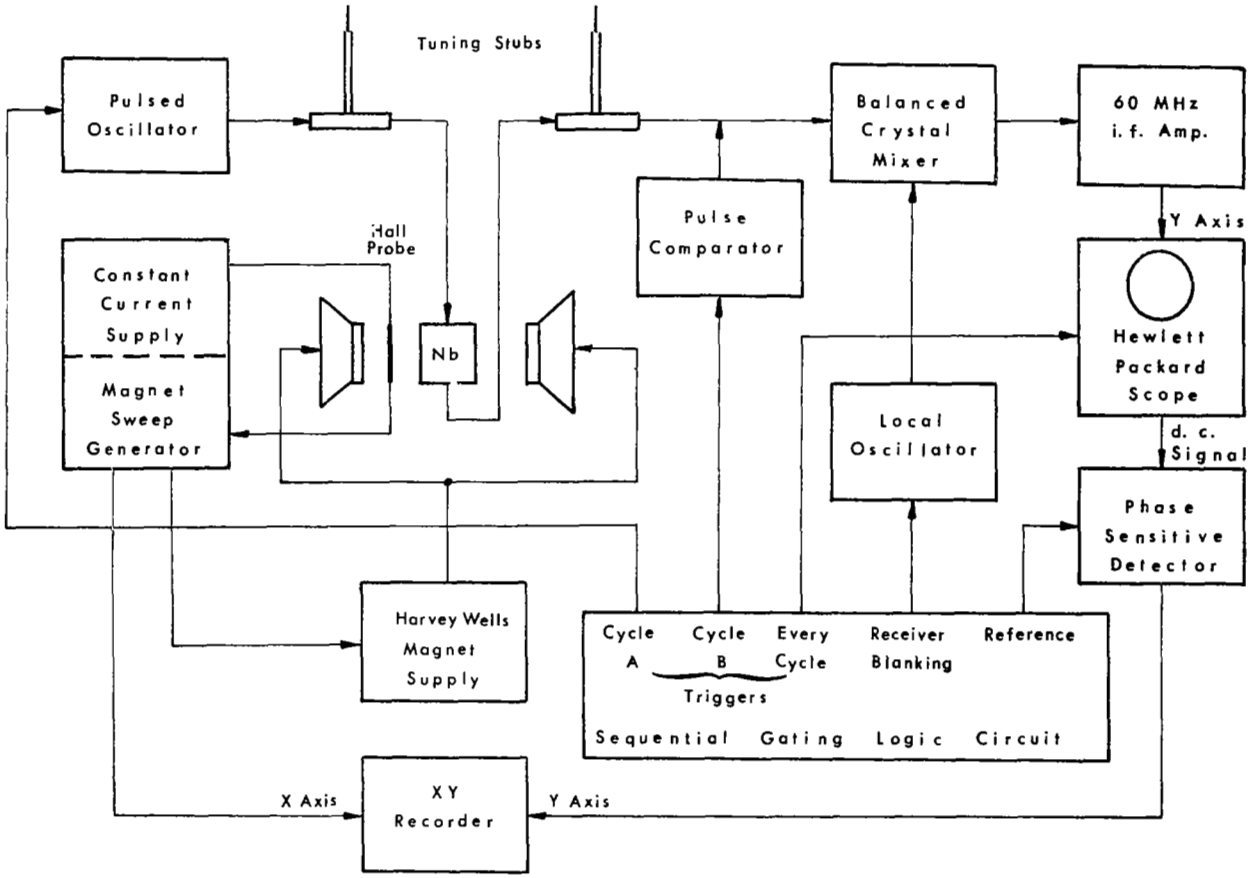

Figure 3. Block diagram of pulse-echo system.

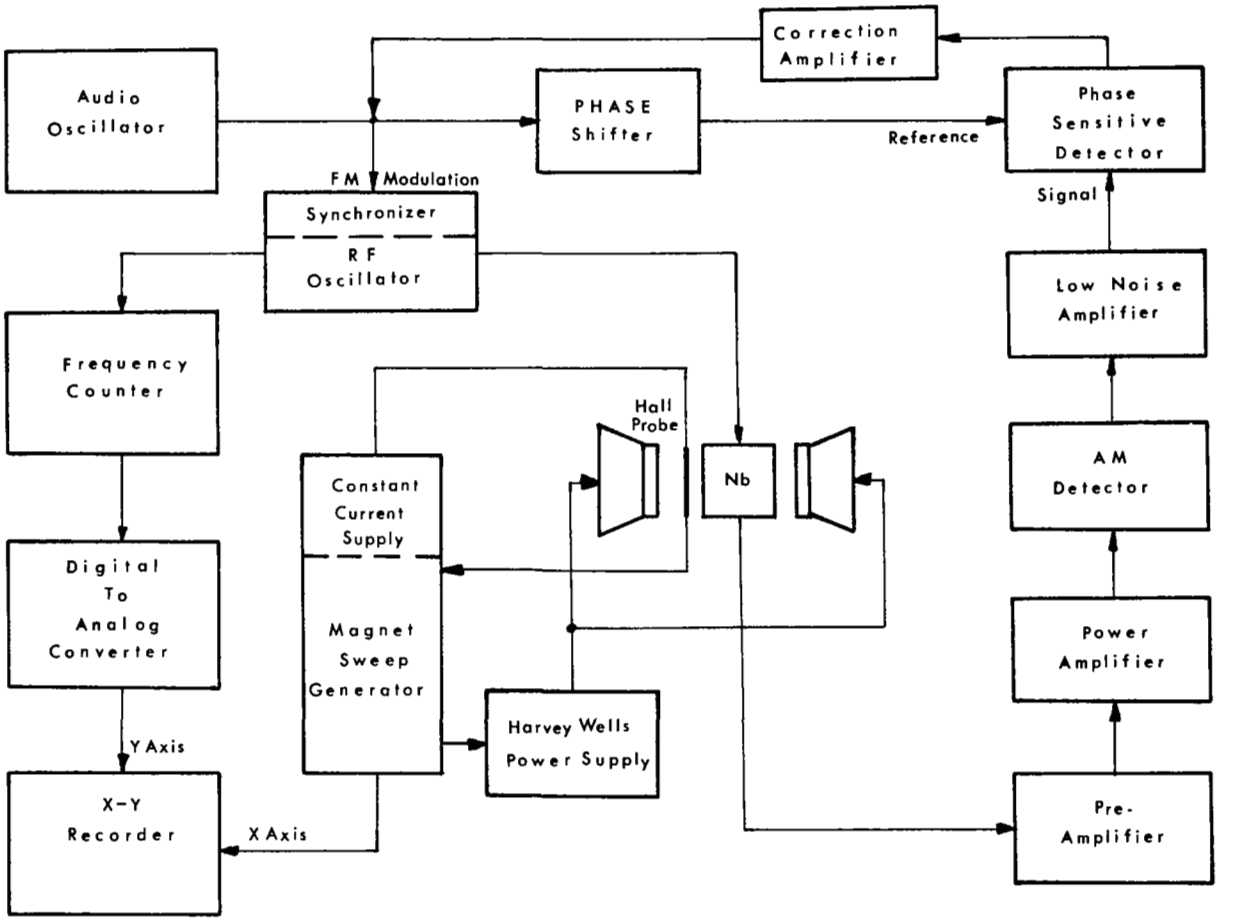

Figure 4. Block diagram of velocity system.

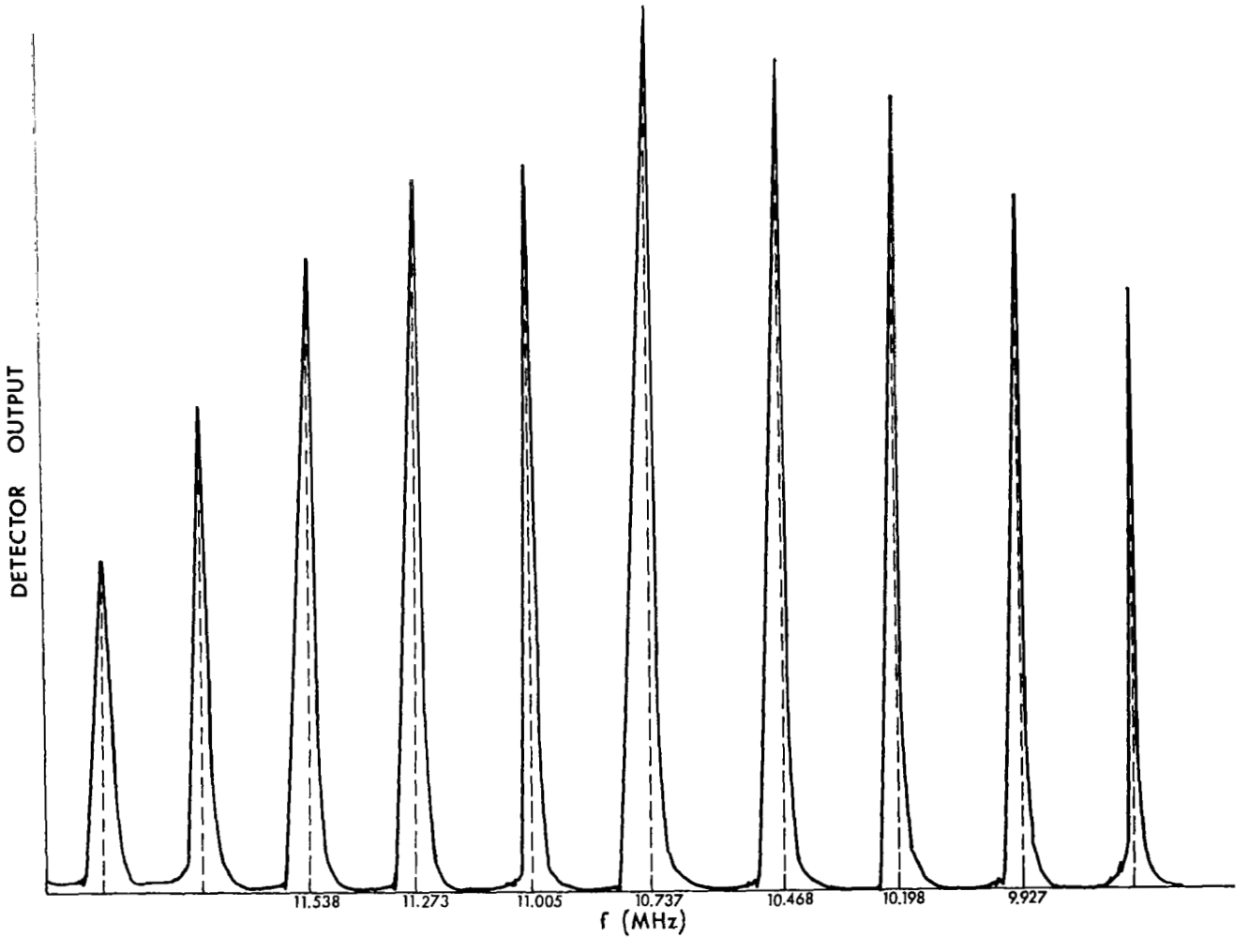

Figure 5. Detector output (relative scale) vs. frequency (in MHz) for longitudinal waves in Nb at 77°K.

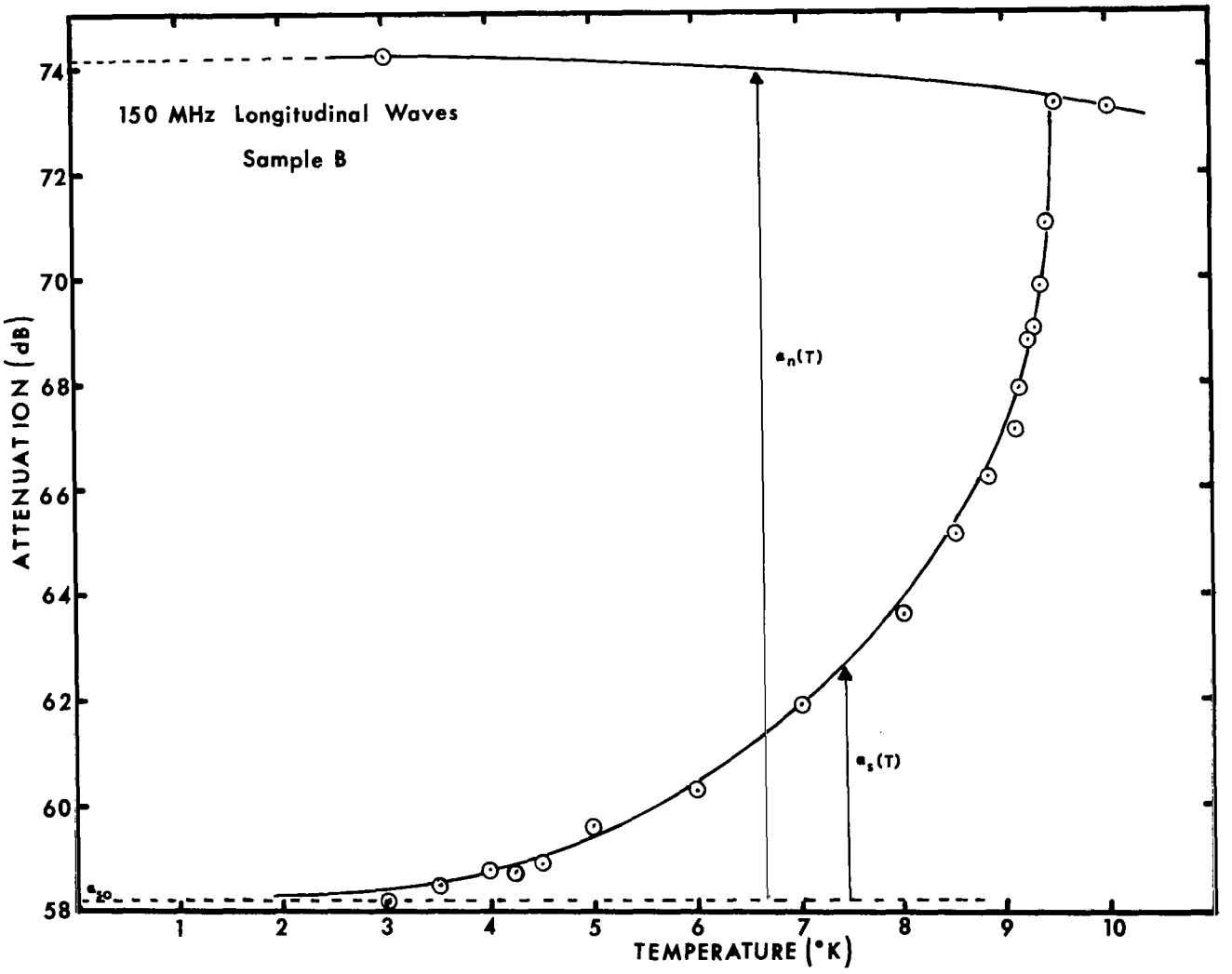

Figure 6. Typical plot of attenuation vs. temperature of 150 MHz longitudinal waves in Sample B along [110].

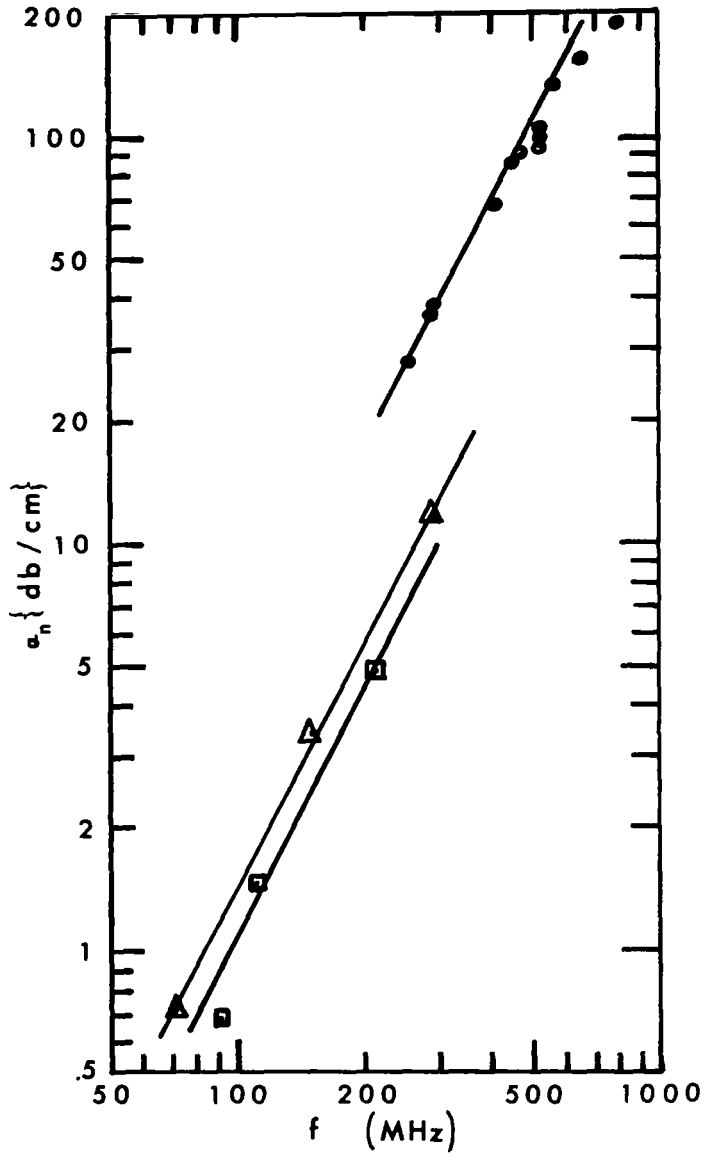

Figure 7. Log α_n vs. log f for longitudinal waves along [110] in Nb. Circles are for Sample A; triangles are for Sample B; squares are for Sample C before annealing. Data for Samples A and B were taken at T = 3.0°K; data for Sample C was taken at T = 4.5°K. Solid lines show f^2 dependence.

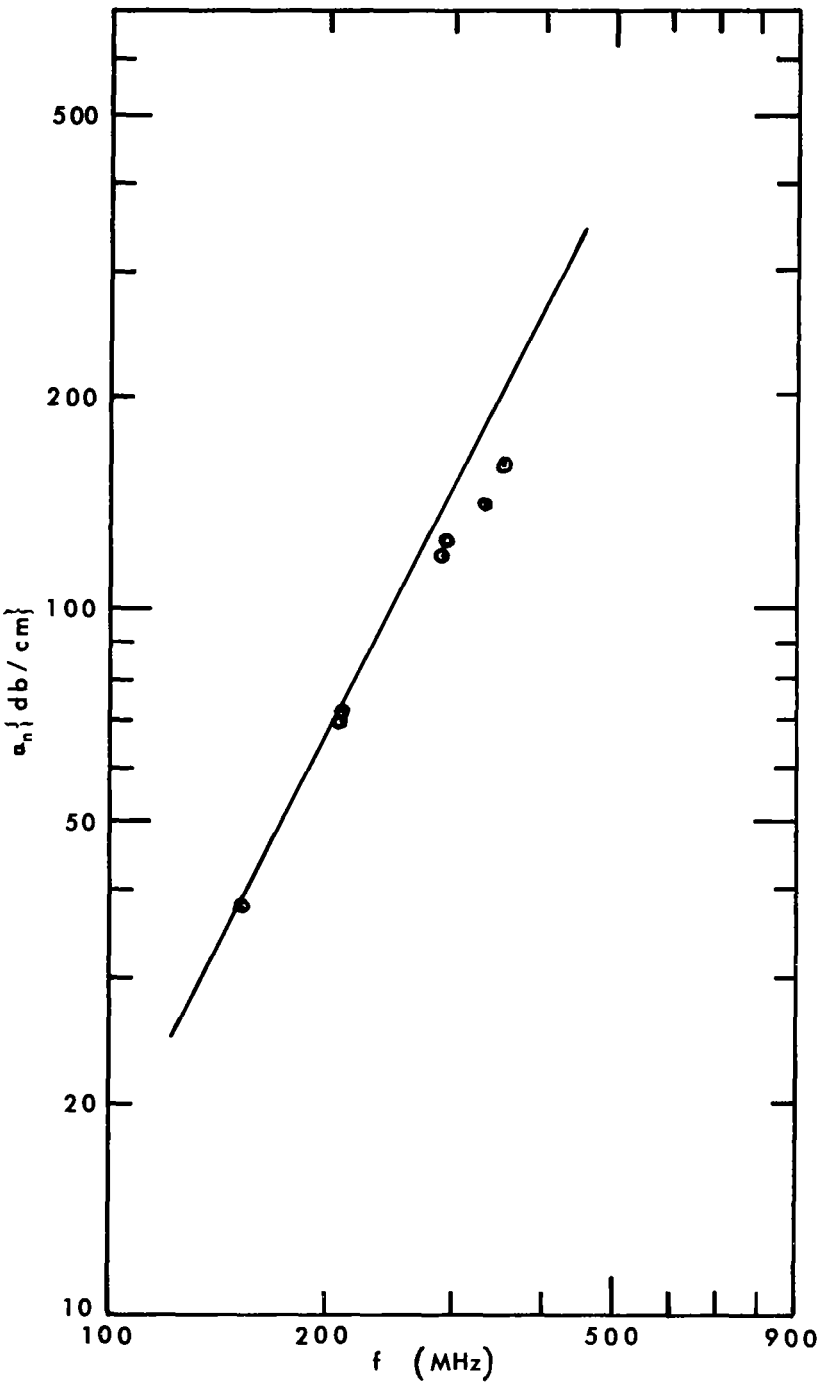

Figure 8. Log α_n vs. log f for transverse (C') waves along the [110] in Nb. Data is from Sample A and was taken at T = 3.0°K. Solid line shows f^2 dependence.

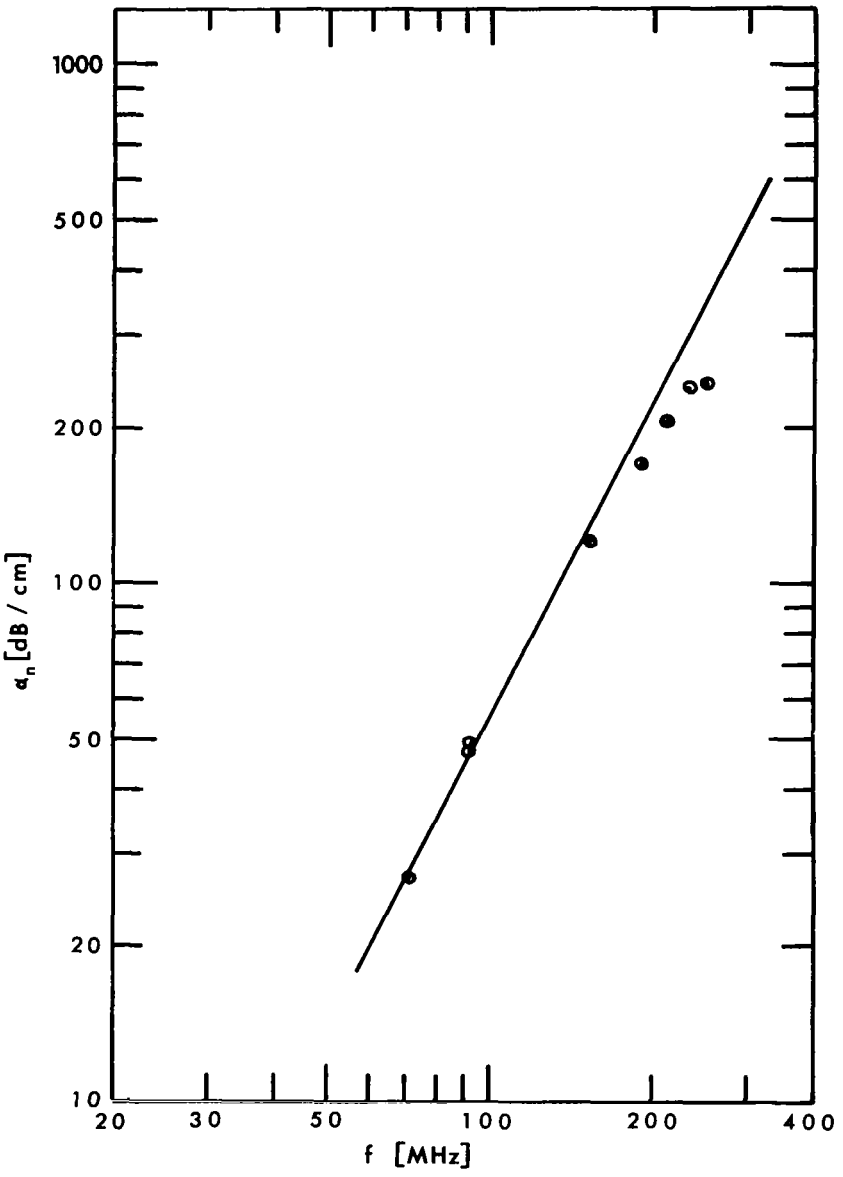

Figure 9. Log α_n vs. log f for transverse (C_{44}) waves along the [110] direction in Nb. Data is from Sample A and was taken at T = 3.0°K. Solid line shows f^2 dependence.

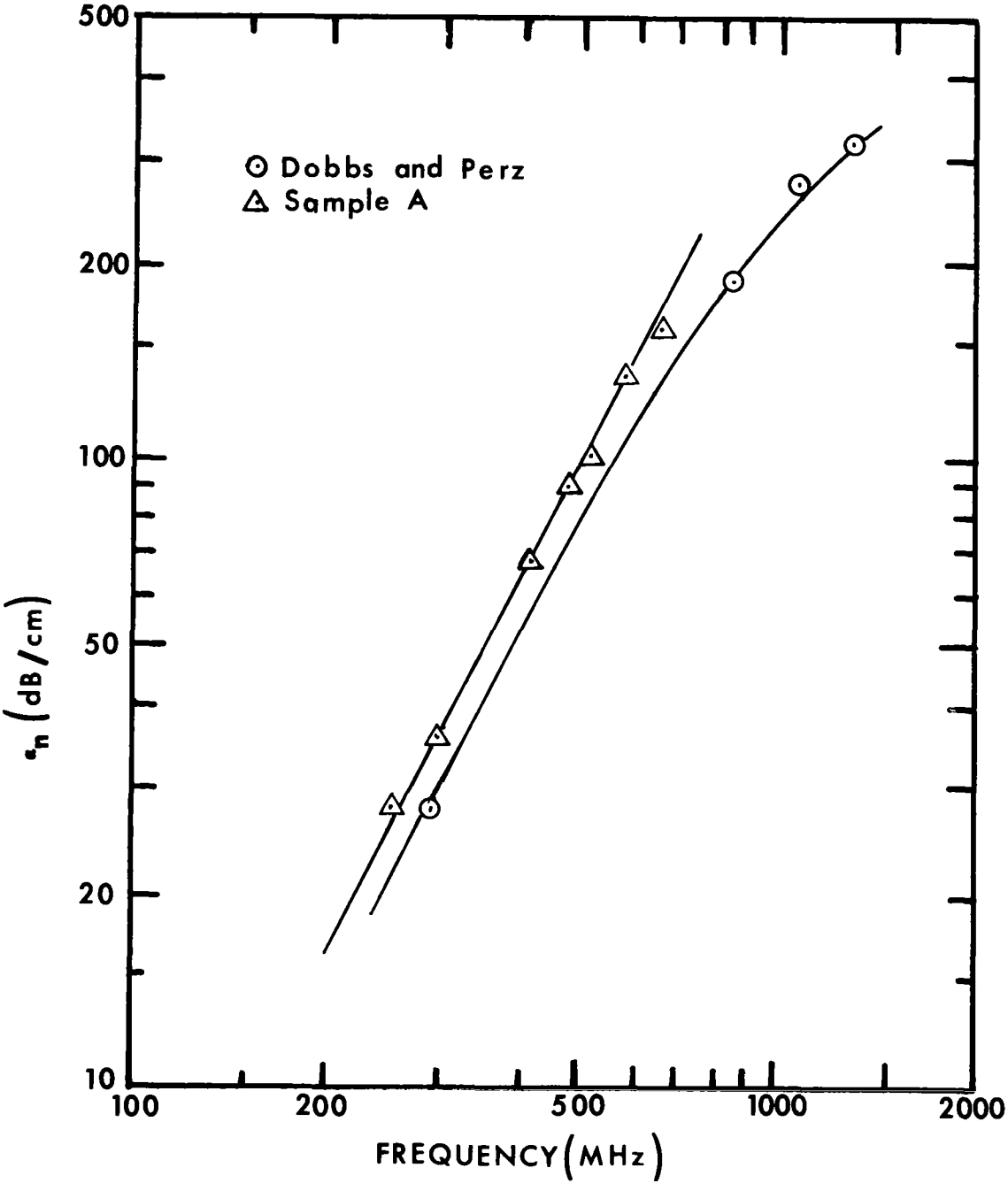

Figure 10. Log α_n vs. log f for longitudinal waves along [110] in Sample A and in sample used by Perz and Dobbs[18]. The straight line shows f^2 dependence.

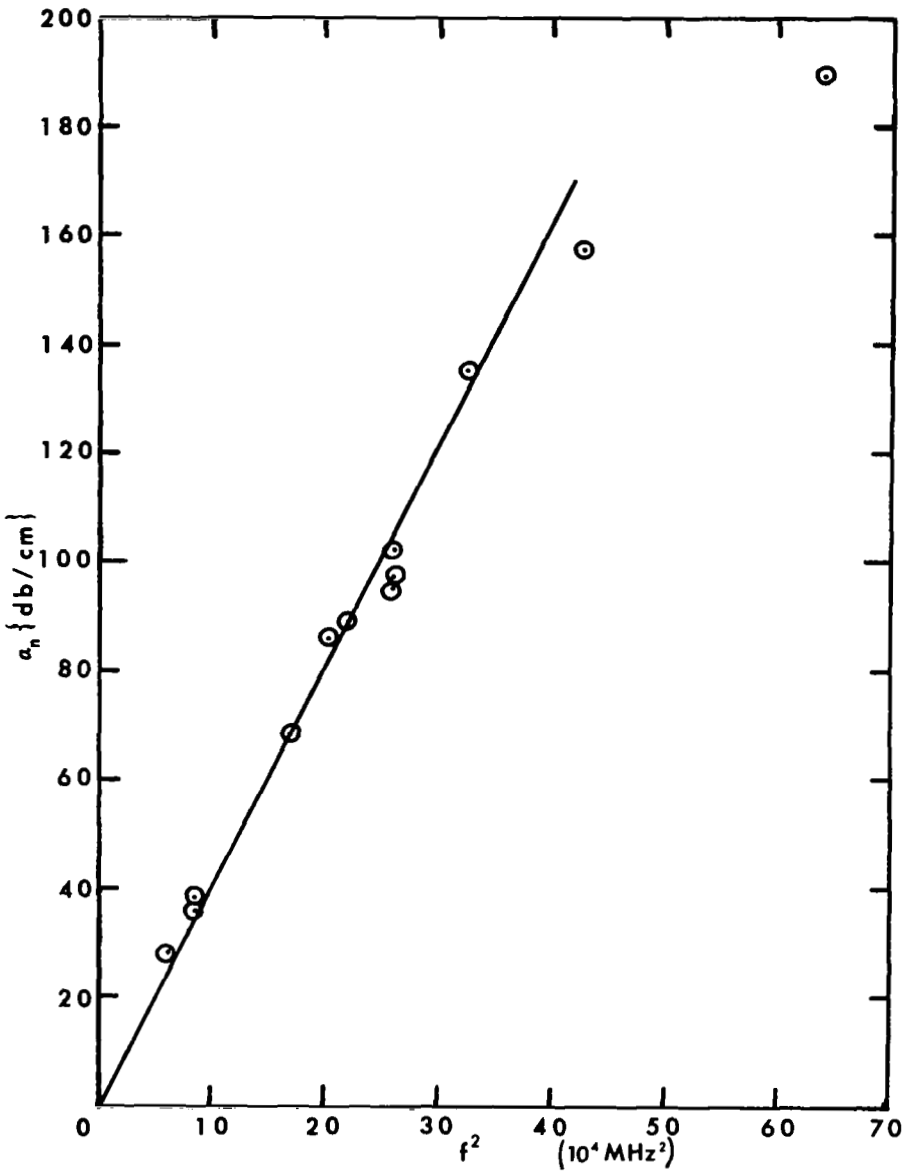

Figure 11. α_n vs. f^2 for longitudinal waves along [110] in Nb showing a deviation of α_n from a frequency squared law at higher frequencies. Data is from Sample A and was taken at T = 3.0°K. Solid line shows f^2 dependence.

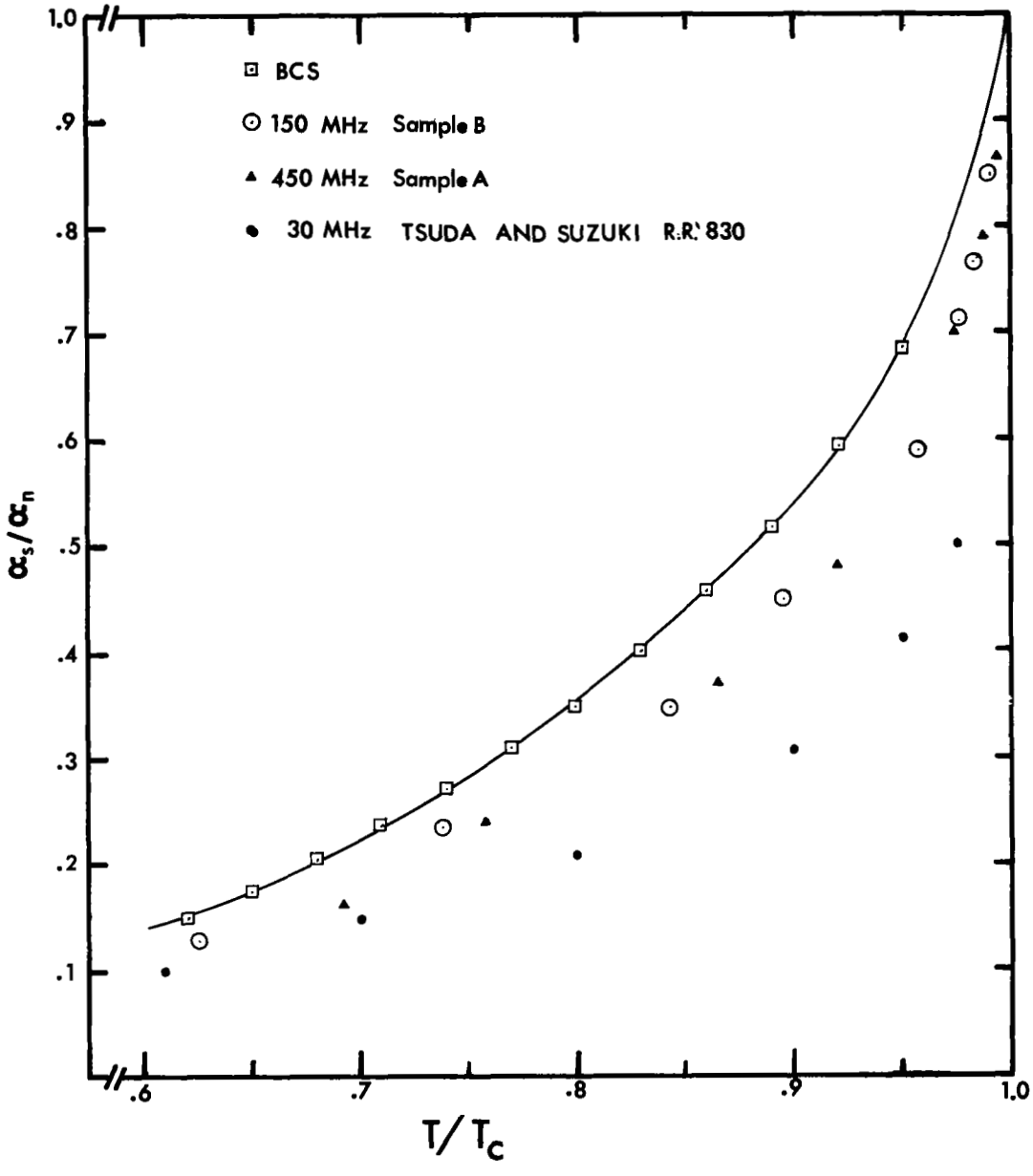

Figure 12. Reduced attenuation vs. reduced temperature for longitudinal waves along [110] in Nb. A BCS curve is shown for comparison. Tsuda and Suzuki data taken from Reference 21.

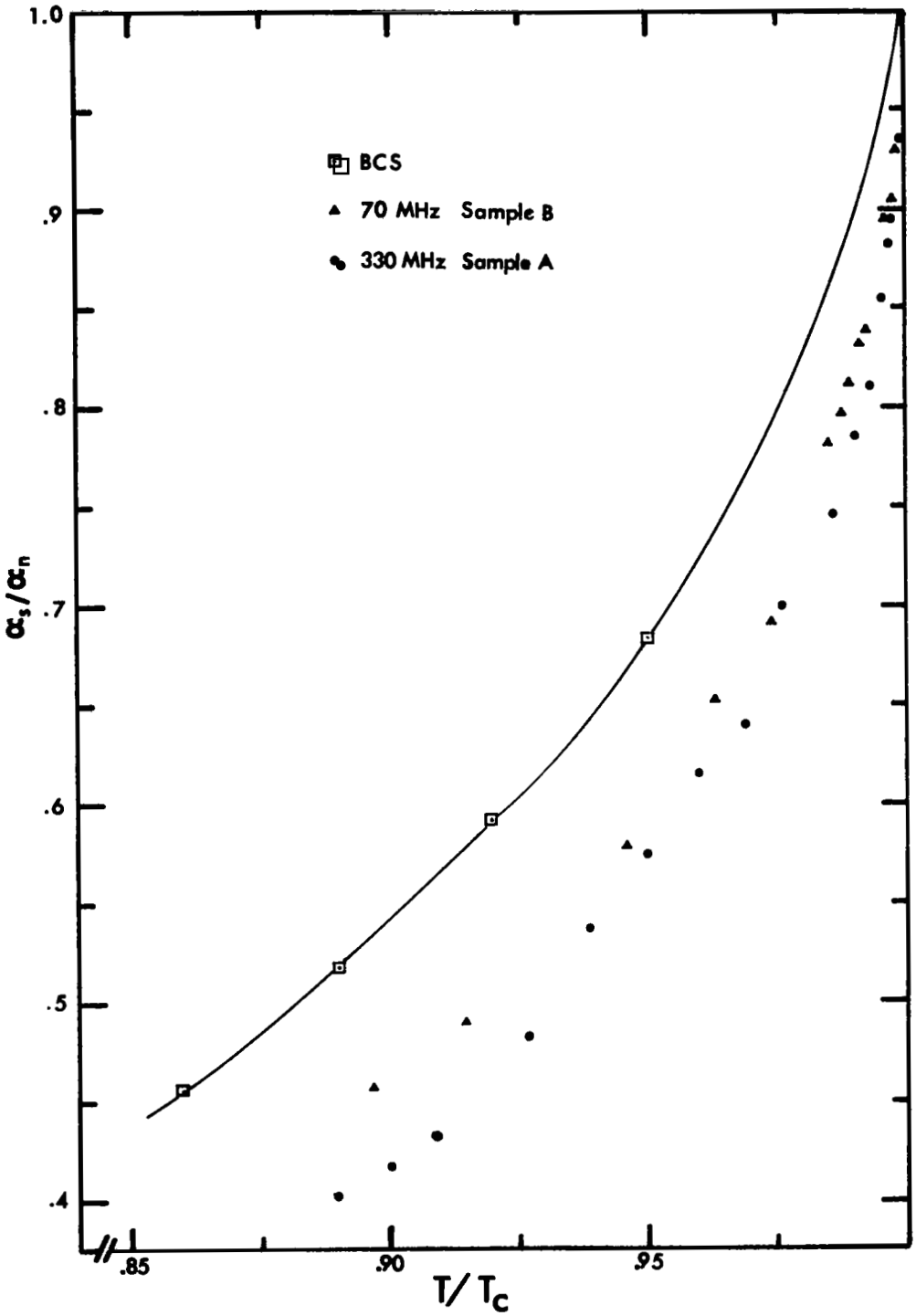

Figure 13. α_s/α_n vs. T/T_c for transverse (C') waves.

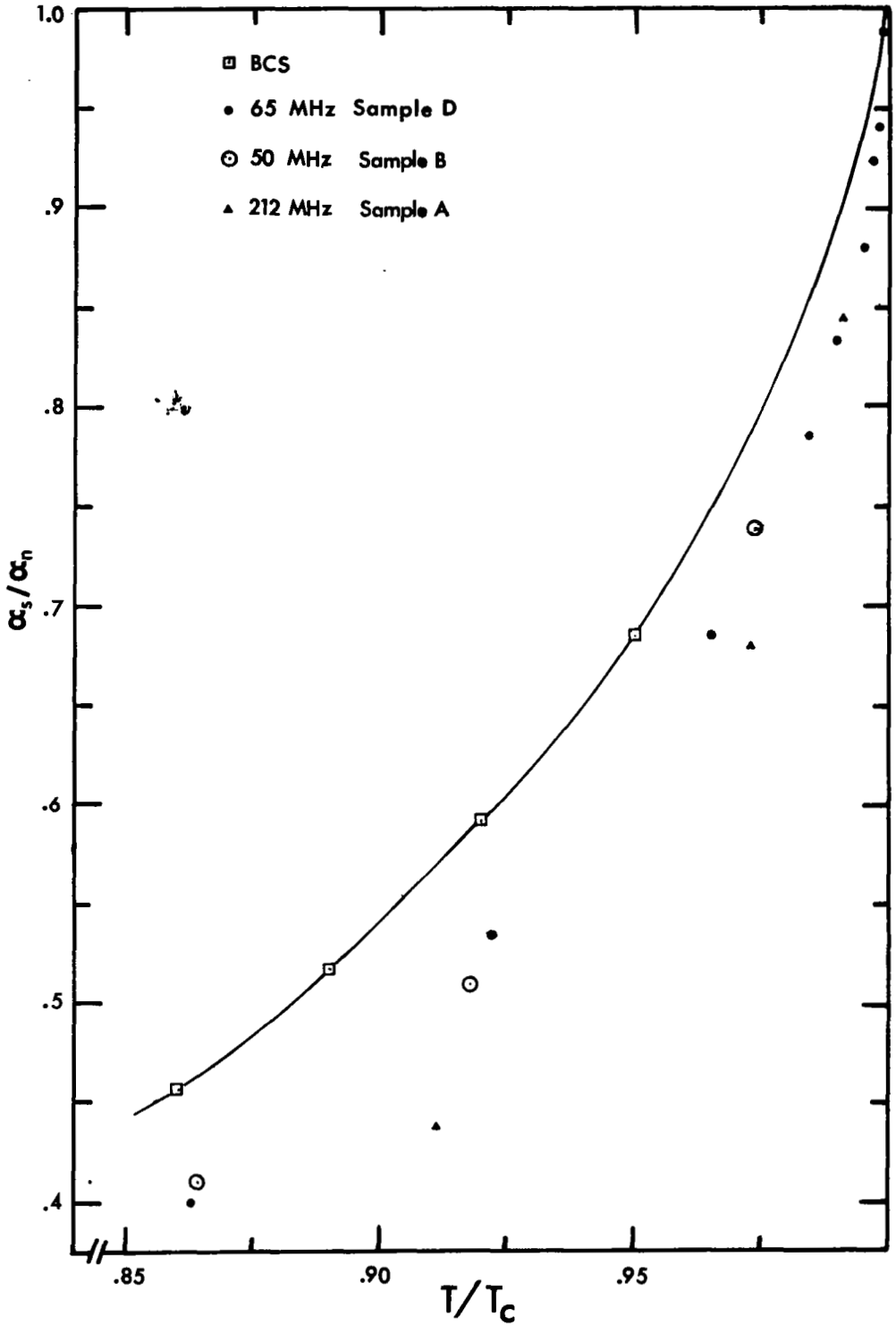

Figure 14. α_s/α_n vs. T/T_c for transverse (C_{44}) waves.

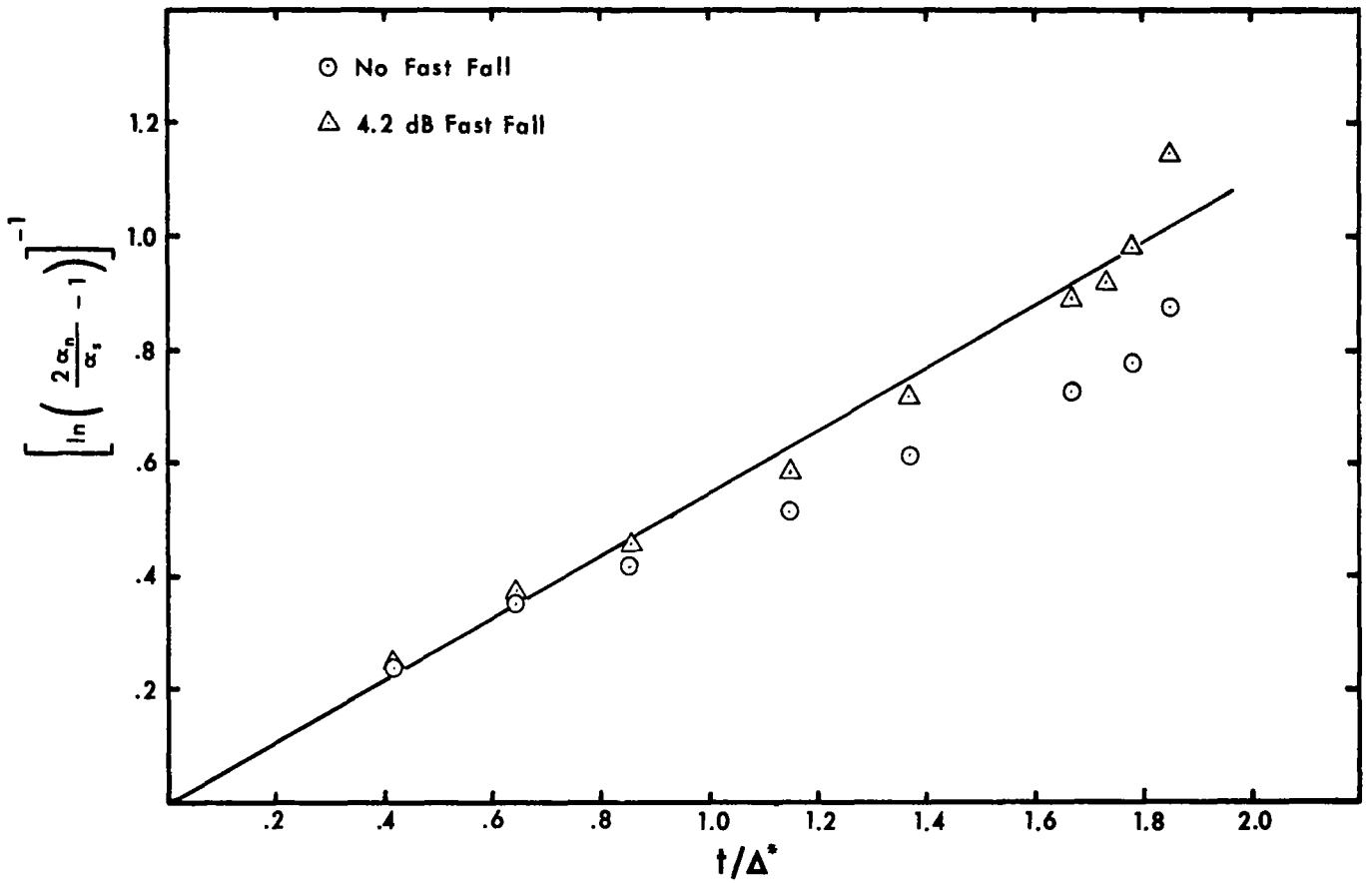

Figure 15. $[\ell n(\frac{2\alpha_n}{\alpha_s} - 1)]^{-1}$ vs. t/Δ^* for 330 MHz transverse (C') waves along [110] in Nb. The data is for Sample A.

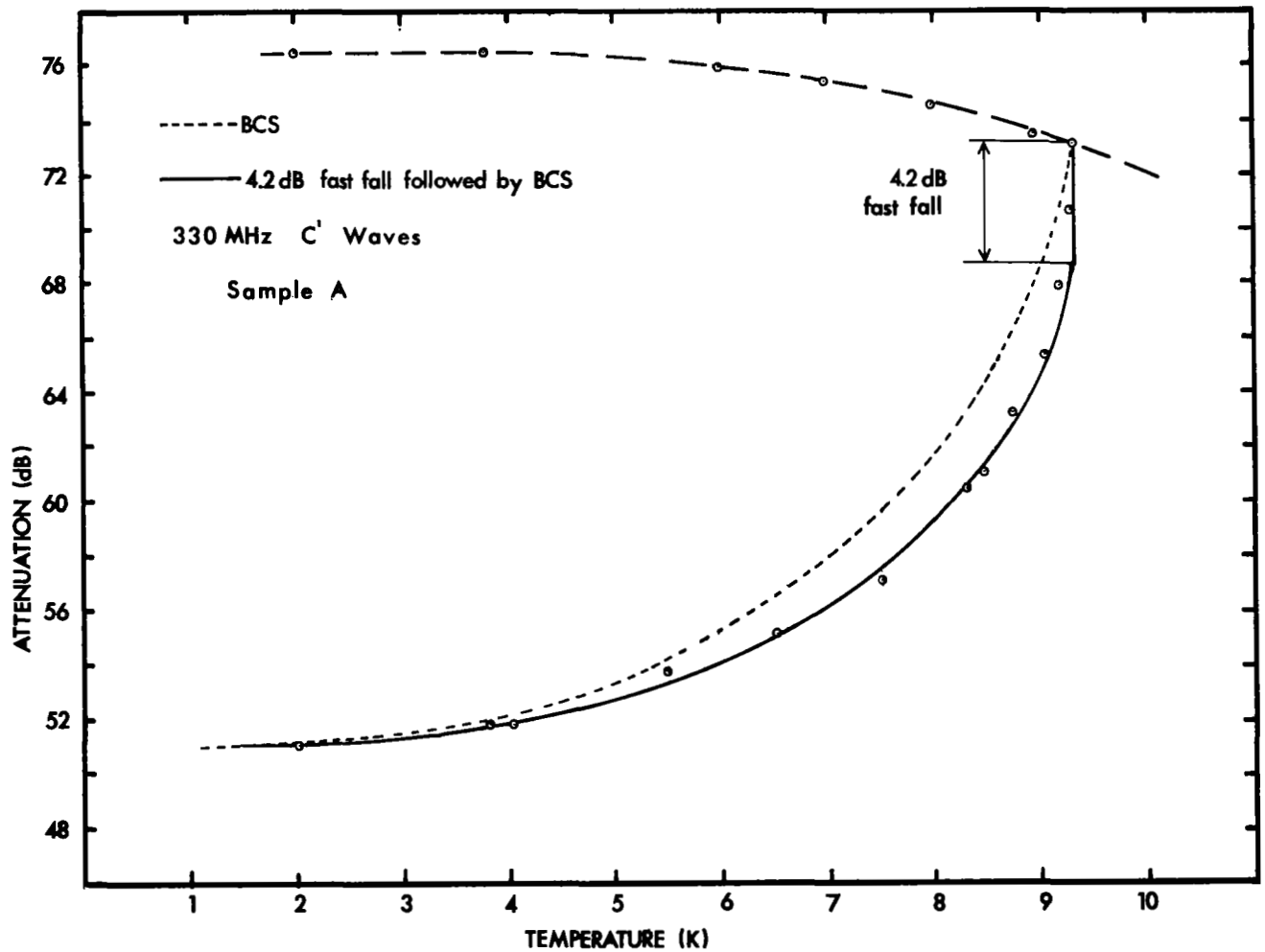

Figure 16. Attenuation vs. temperature for a 330 MHz transverse (C') wave along [110] in Nb.

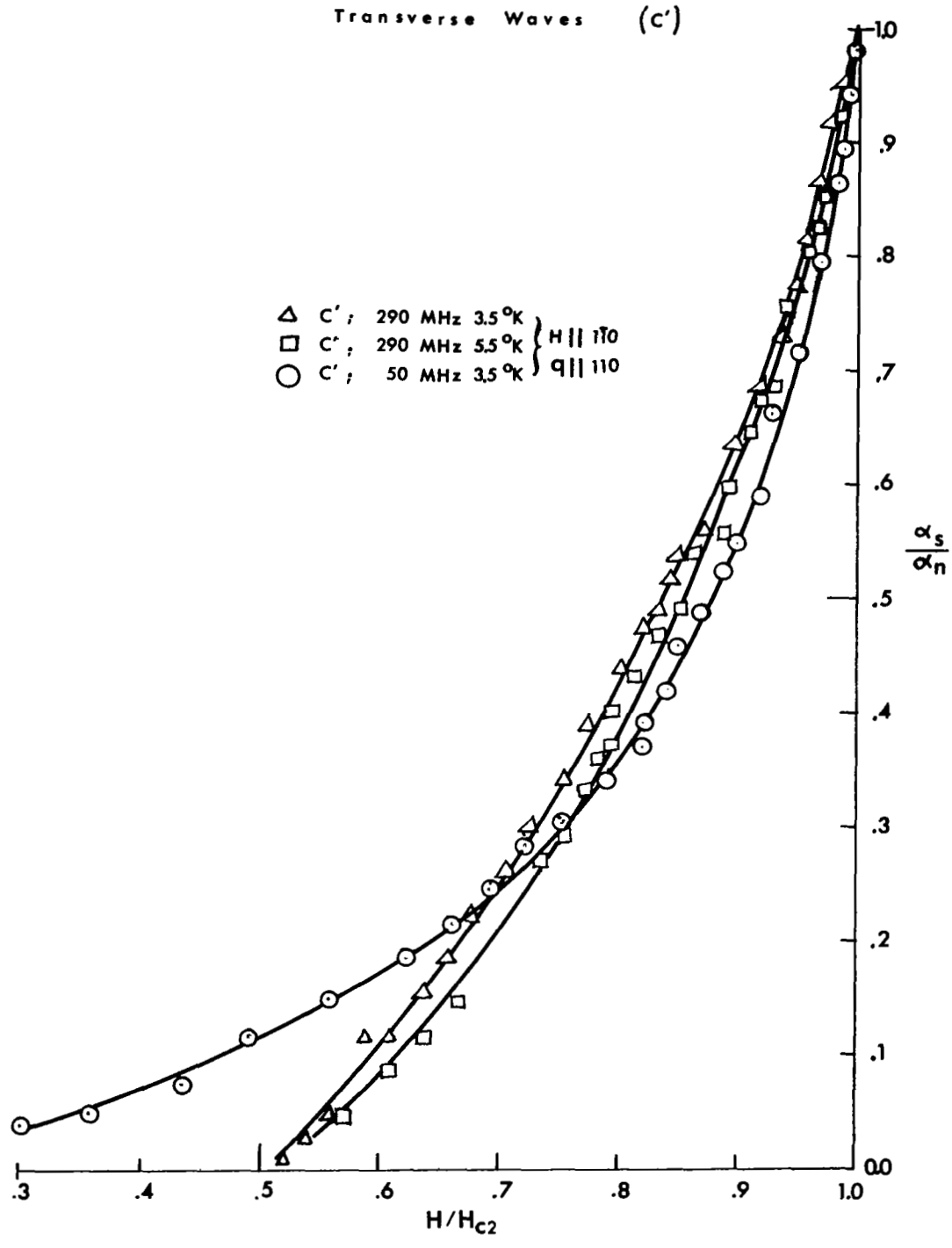

Figure 17. α_s/α_n vs. H/H_{c2} for transverse (C') waves in Nb. The 290 MHz data is for Sample A and the 50 MHz data is for Sample B.

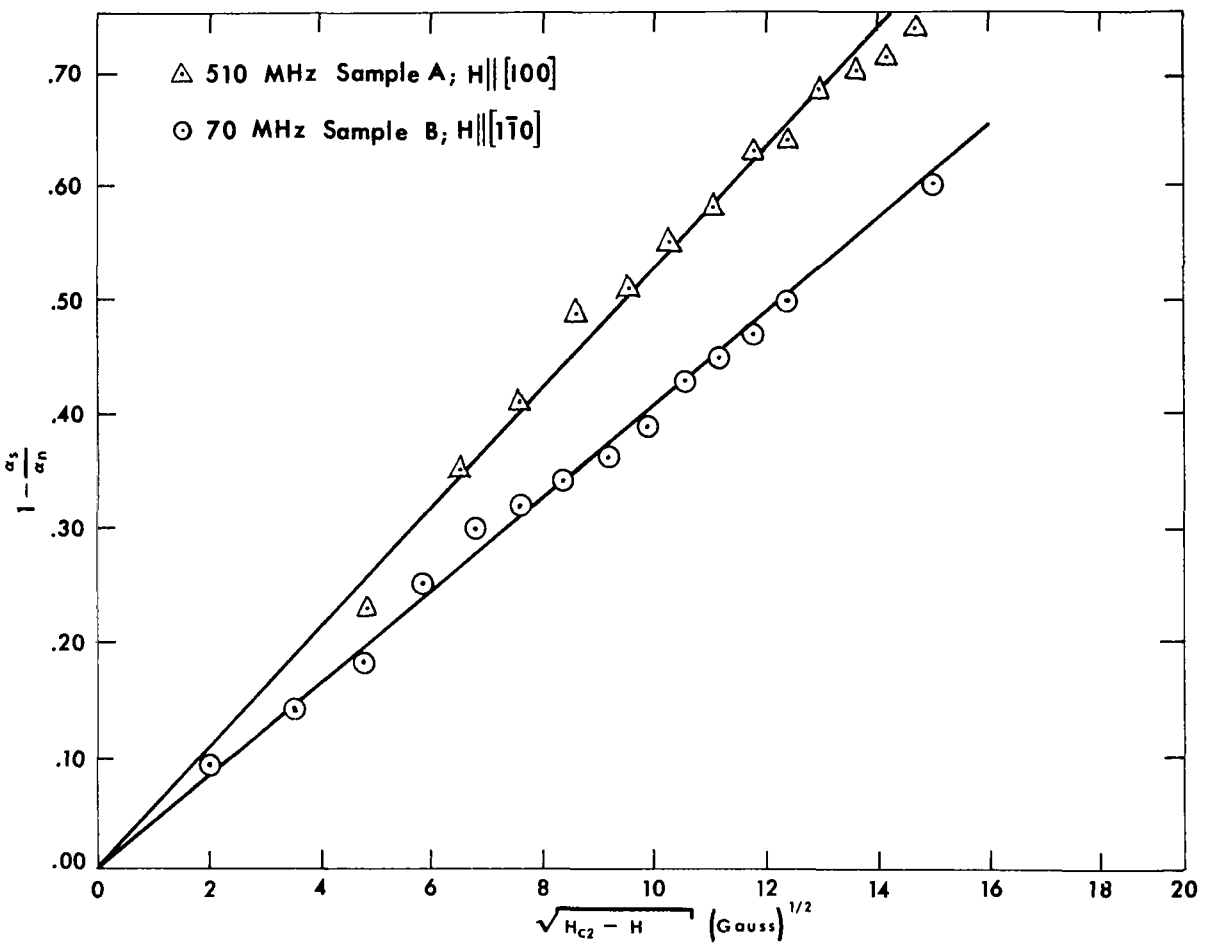

Figure 18. $1-\frac{\alpha_s}{\alpha_n}$ vs. $(H_{c2}-H)^{1/2}$ for longitudinal waves along [110] in Nb at 3.5°K.

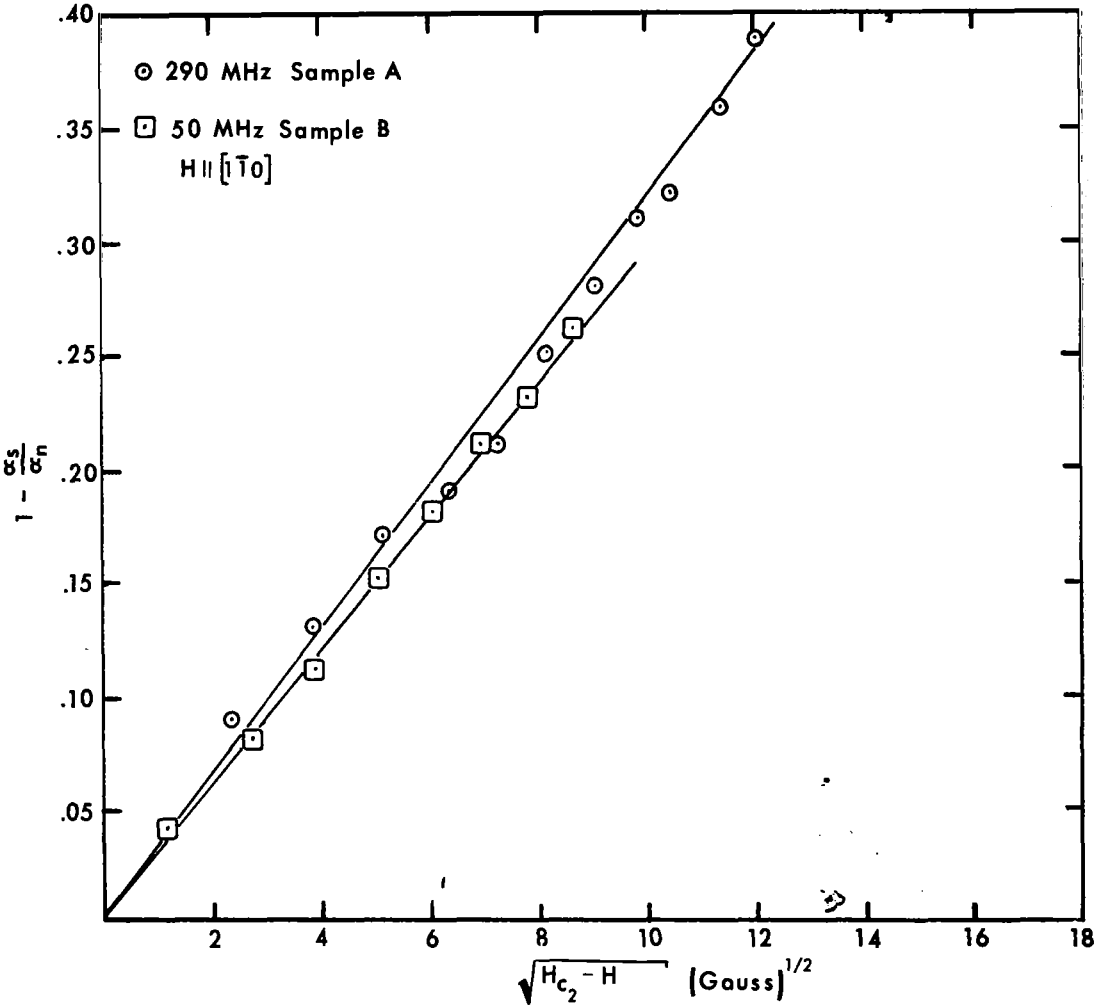

Figure 19. $1 - \frac{\alpha_s}{\alpha_n}$ vs. $(H_{c2}-H)^{1/2}$ for transverse (C') waves along [110] in Nb at 3.5°K.

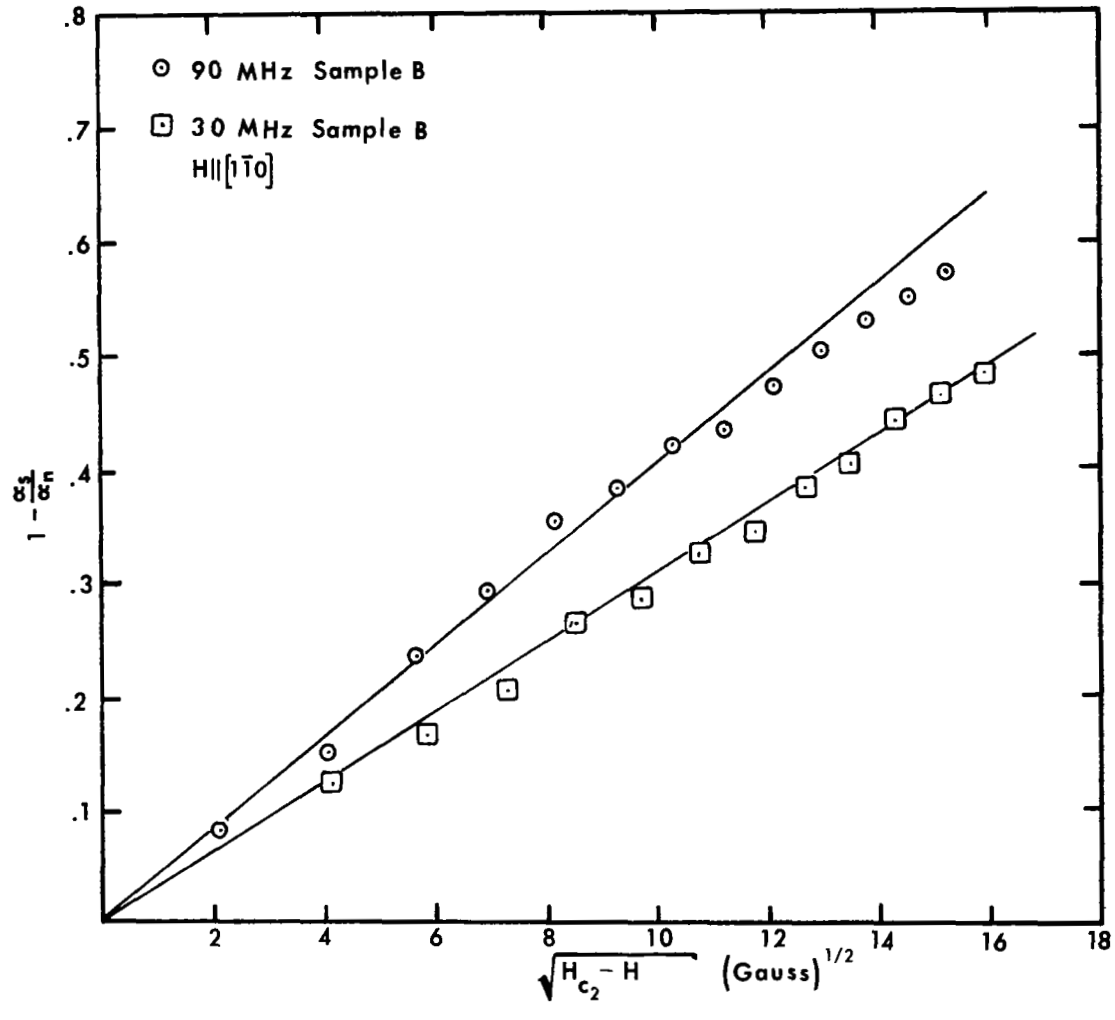

Figure 20. $1-\frac{\alpha_s}{\alpha_n}$ vs. $(H_{c2}-H)^{1/2}$ for transverse (C_{44}) waves along [110] in Nb at 3.5°K.

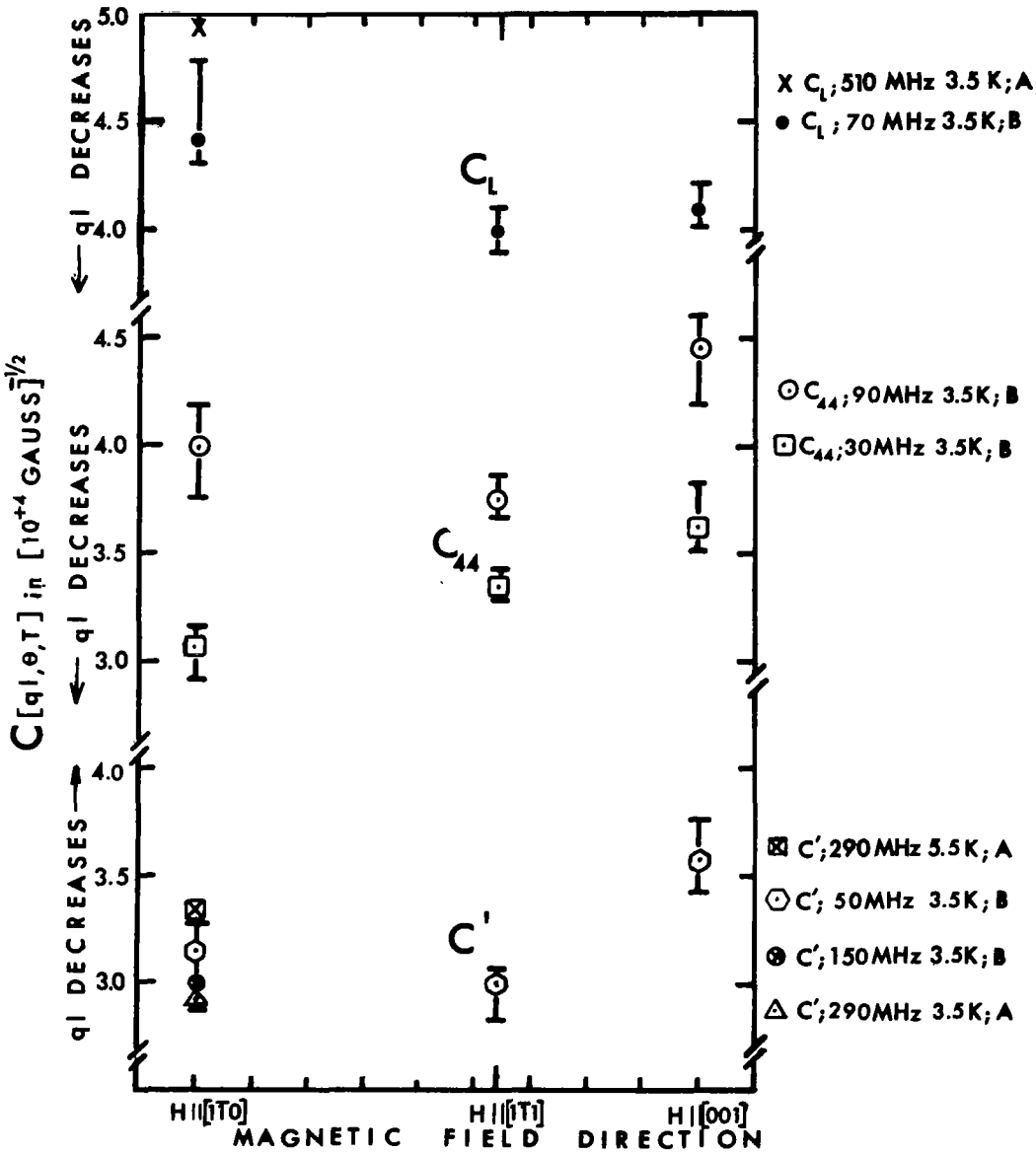

Figure 21. Maki slope vs. magnetic field direction for H perpendicular to plane of q in Nb.

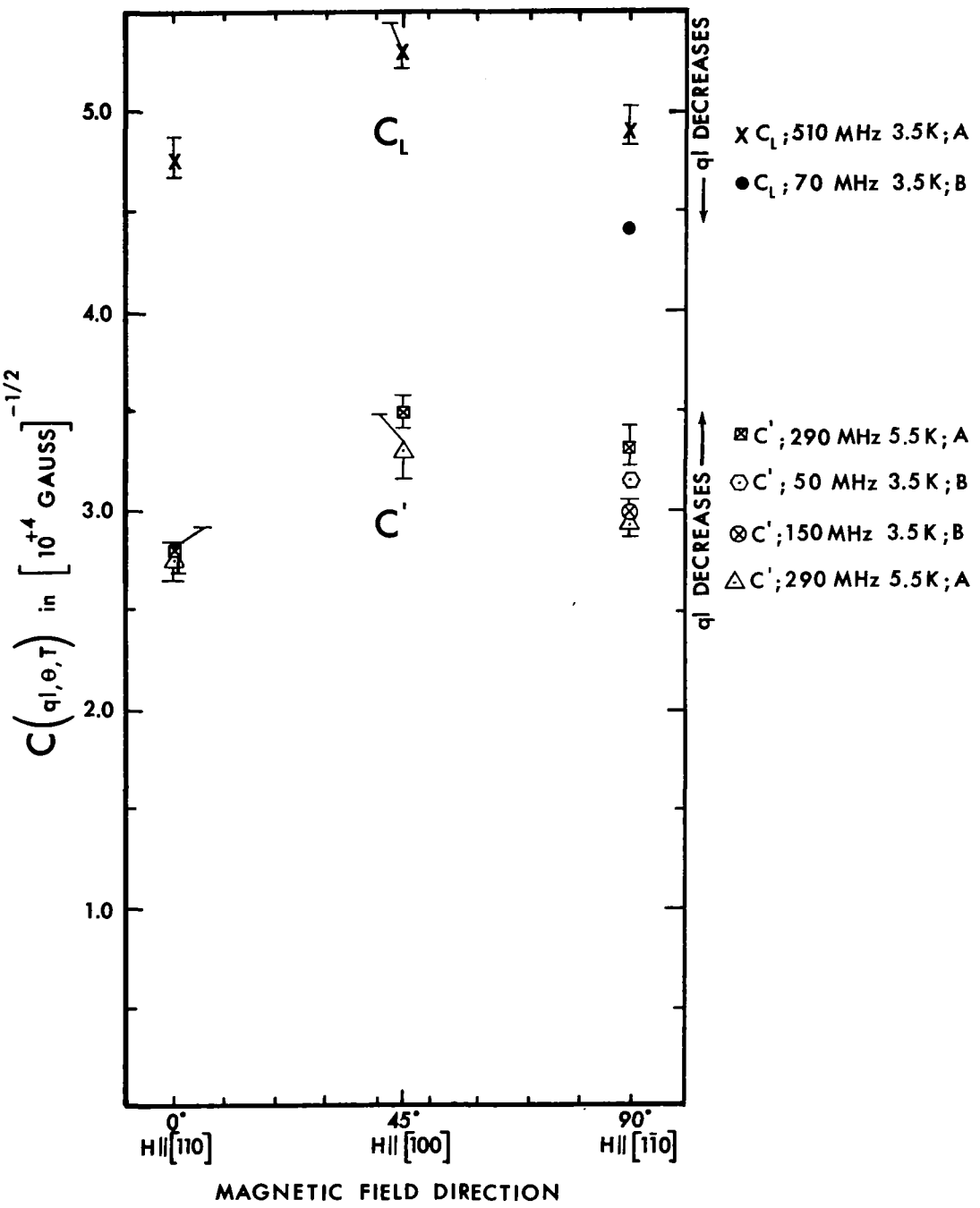

Figure 22. Maki slope vs. magnetic field direction for H in plane of q in Nb.

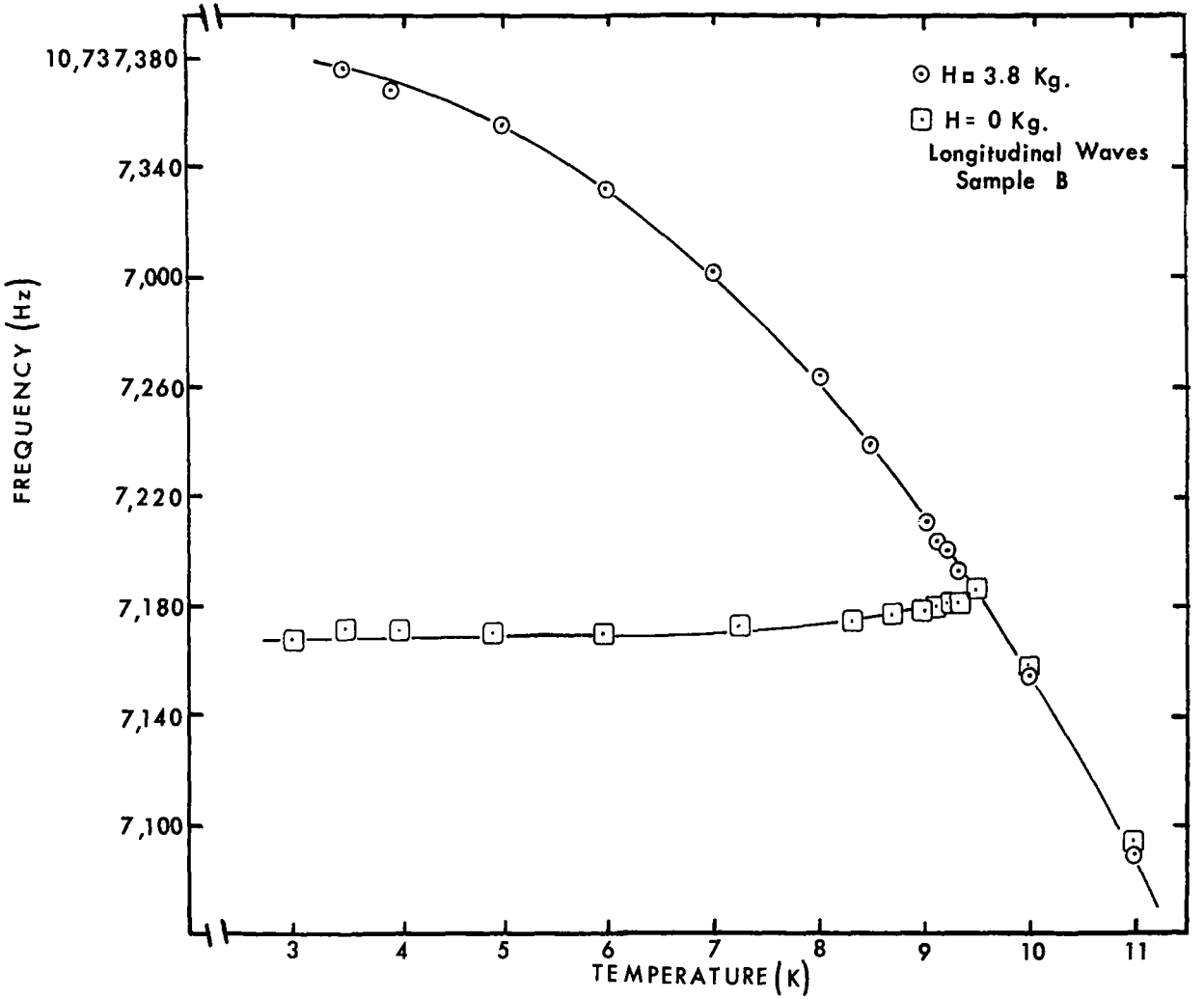

Figure 23. Frequency vs. temperature for longitudinal waves along [110] in Sample B.

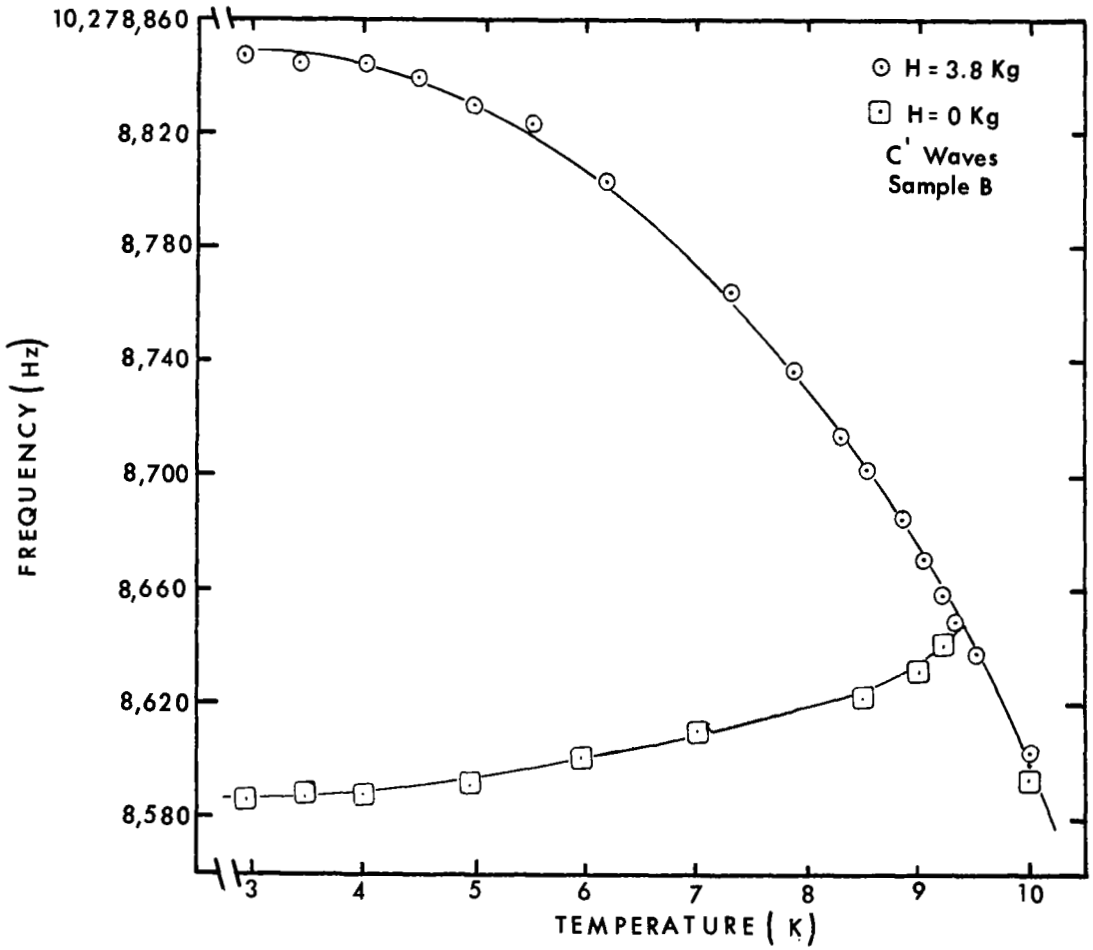

Figure 24. Frequency vs. temperature for transverse (C') waves along [110] in Sample B.

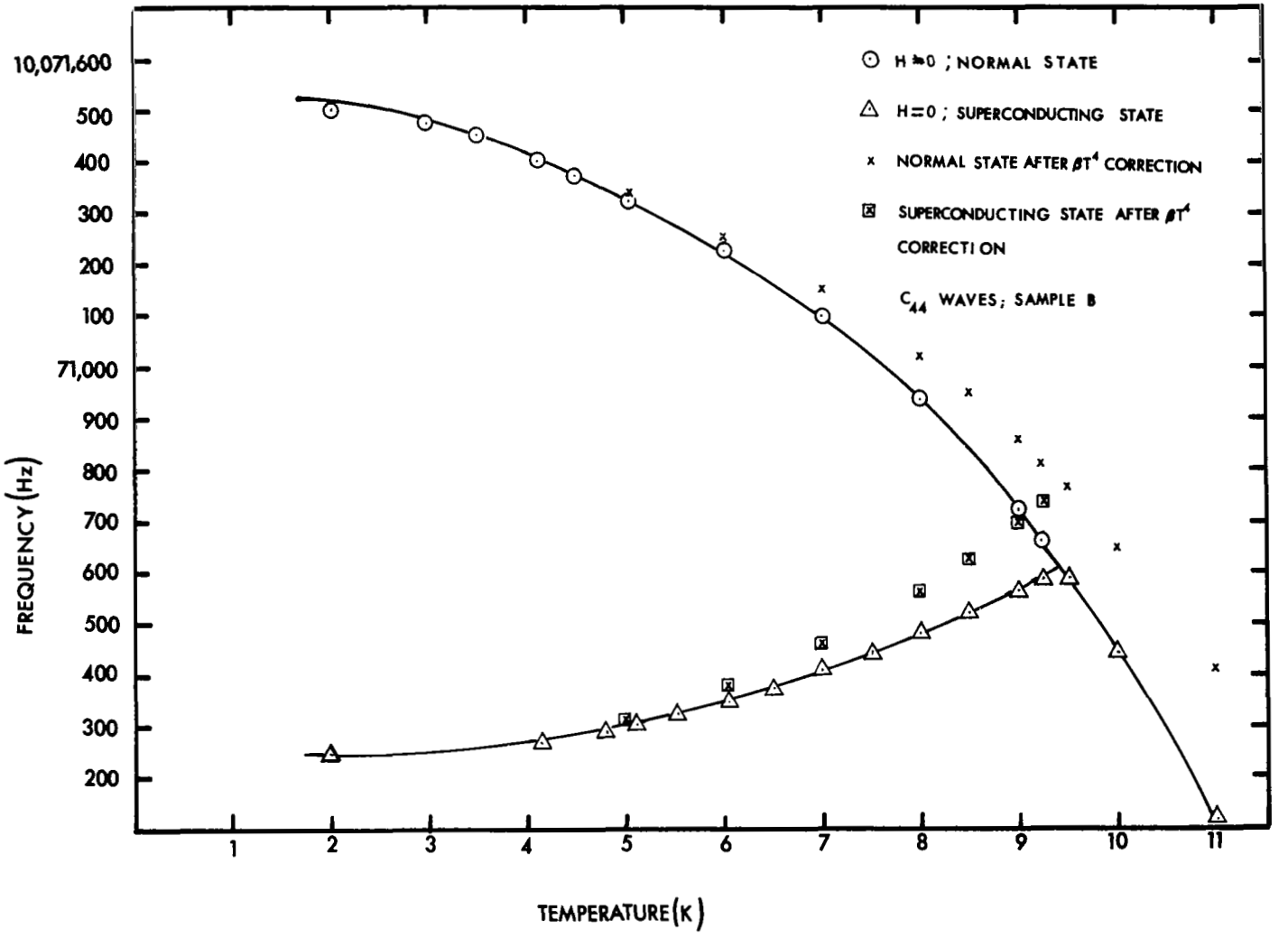

Figure 25. Frequency vs. temperature for transverse (C_{44}) waves along [110] in Sample B.

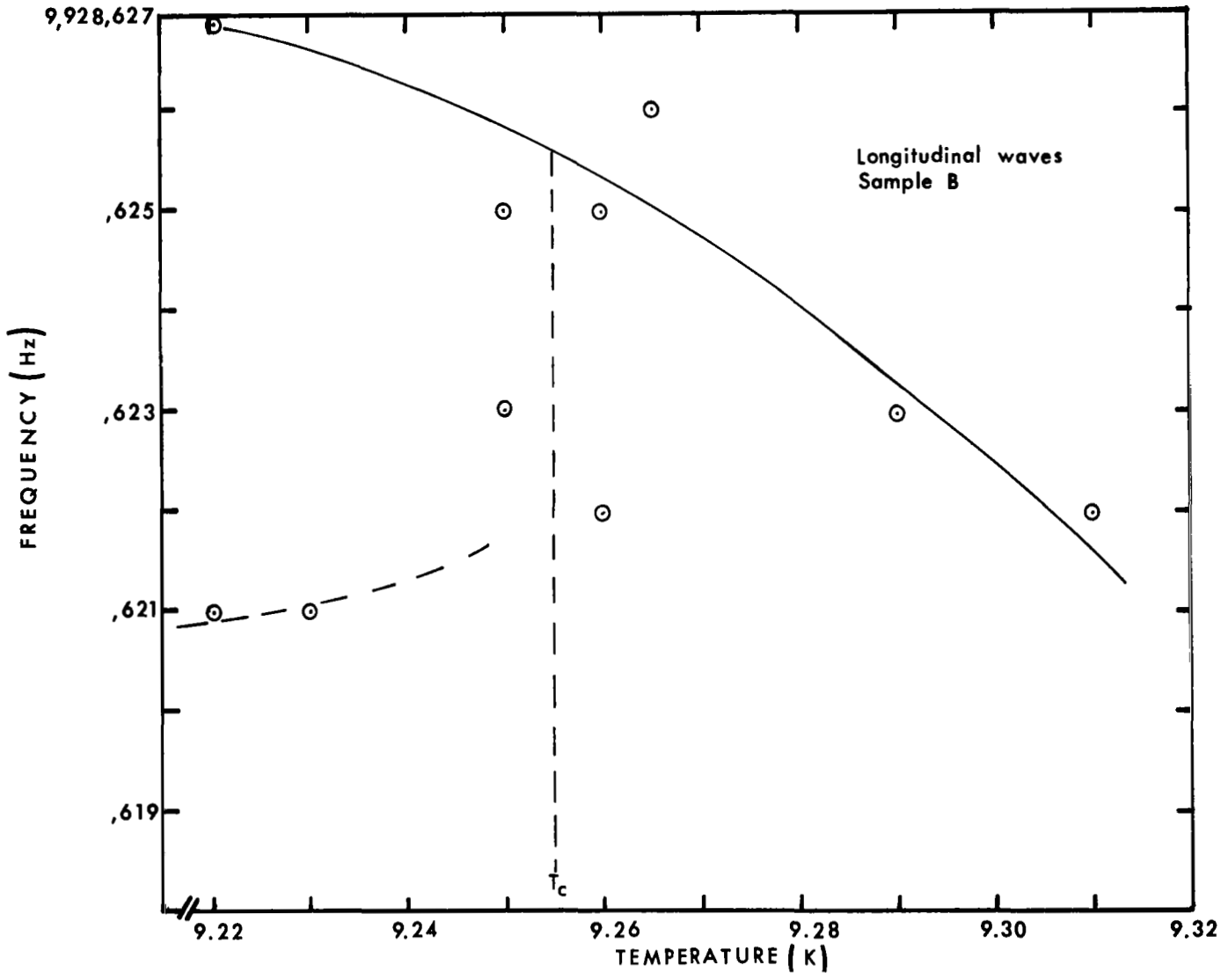

Figure 26. Frequency vs. temperature for longitudinal waves in Sample B near T_c.

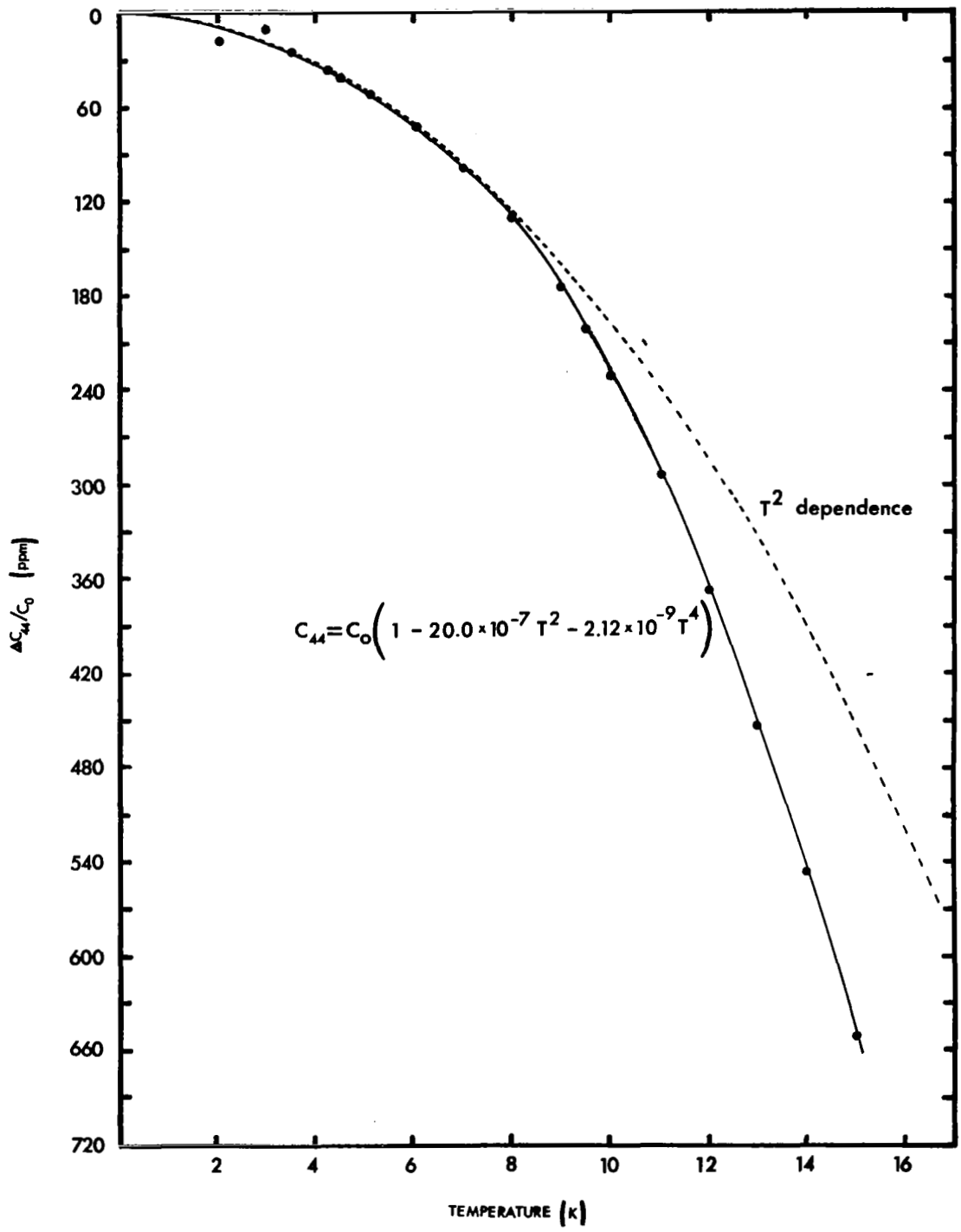

Figure 27. The fractional change in the C_{44} modulus, $\frac{C_{44}}{C_o}$, vs. temperature for Sample B. The dotted line indicates a T^2 dependence only.

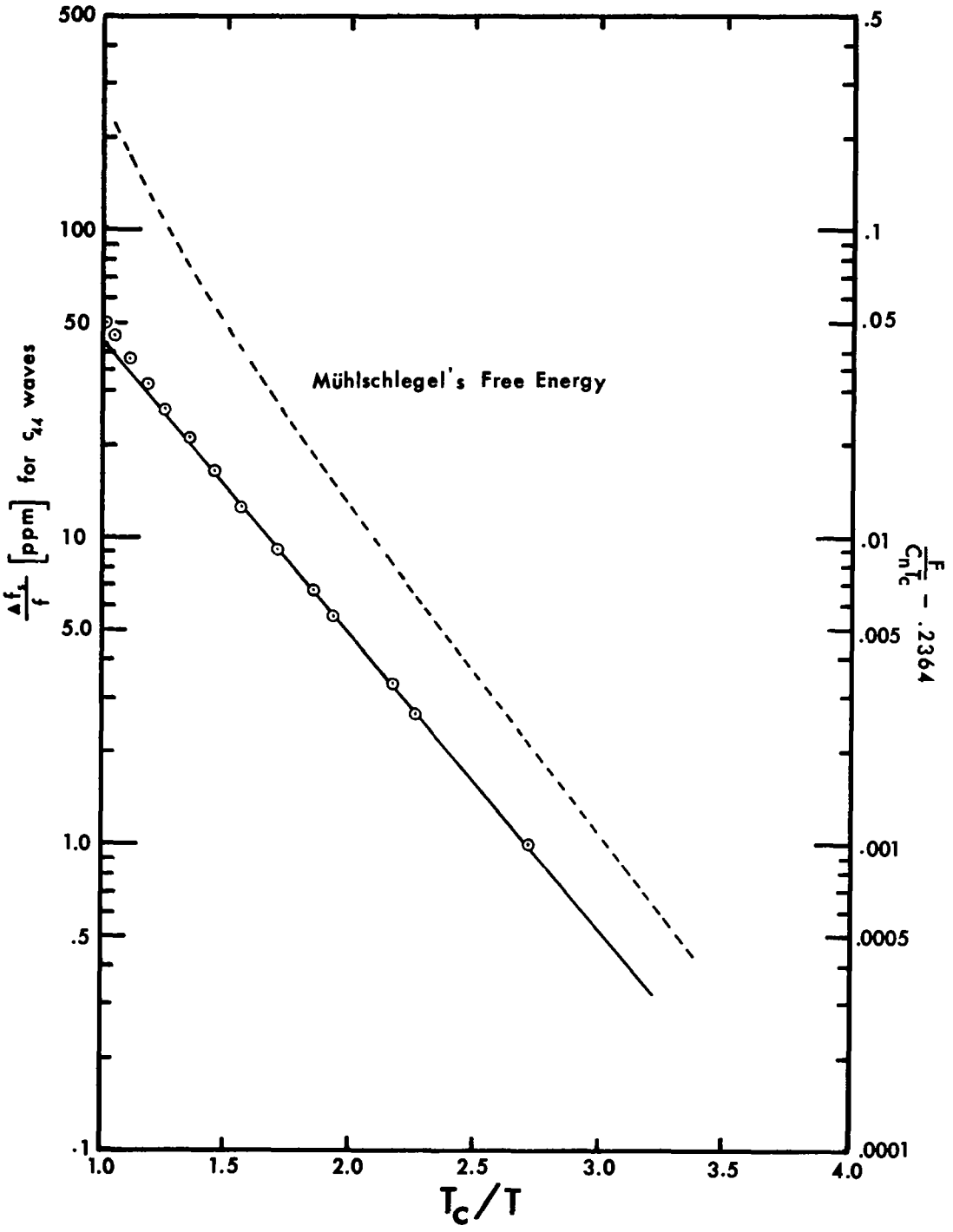

Figure 28. The fractional change of the frequency in the superconducting state, $\frac{\Delta f_s}{f}$, vs. T_c/T in Sample B. The dotted line shows the temperature dependence of the free energy given by Reference 32 as a function of T_c/T.

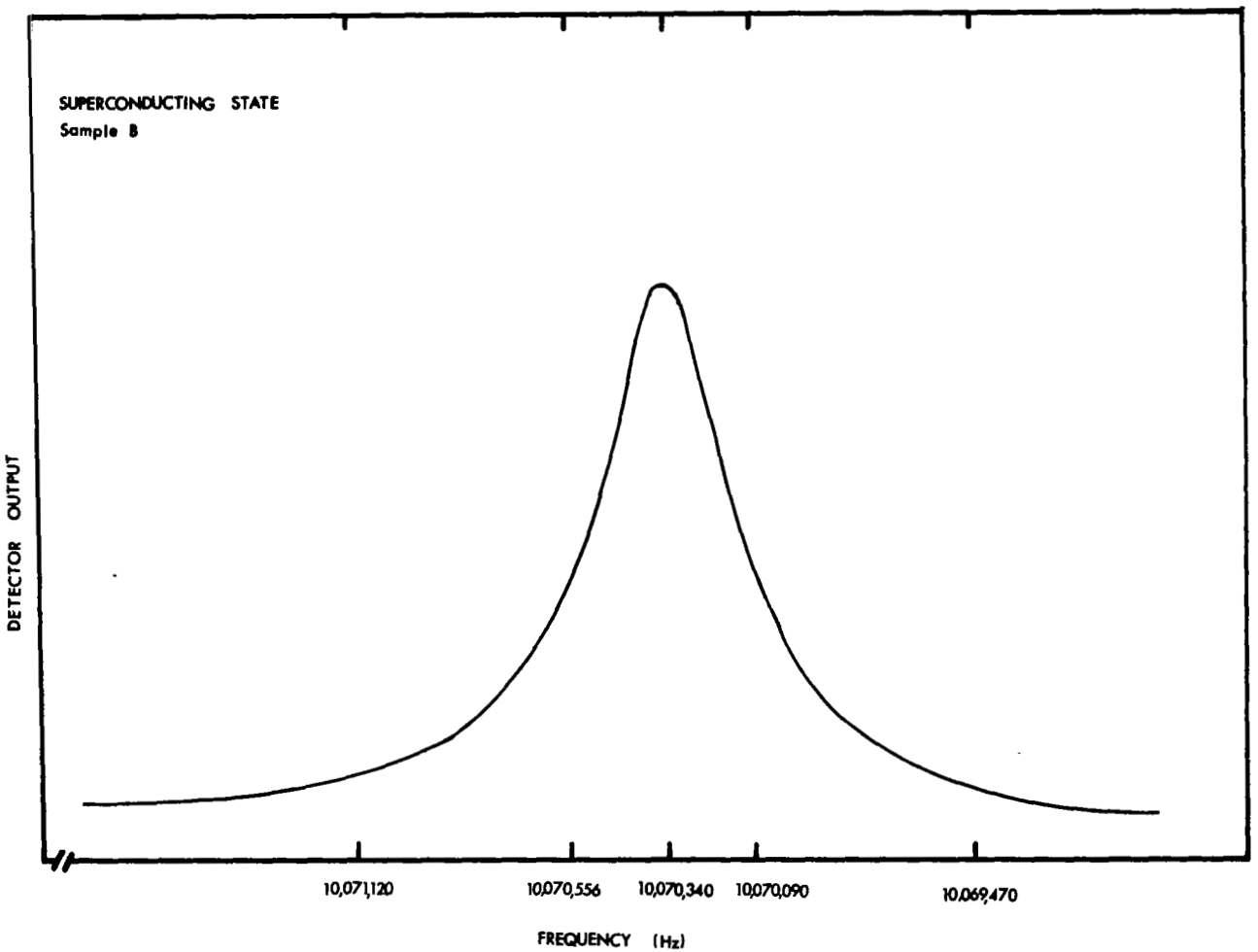

Figure 29. Detector output (arbitrary scale) vs. frequency in the superconducting state for C_{44} transverse waves in Sample B at 4 K.

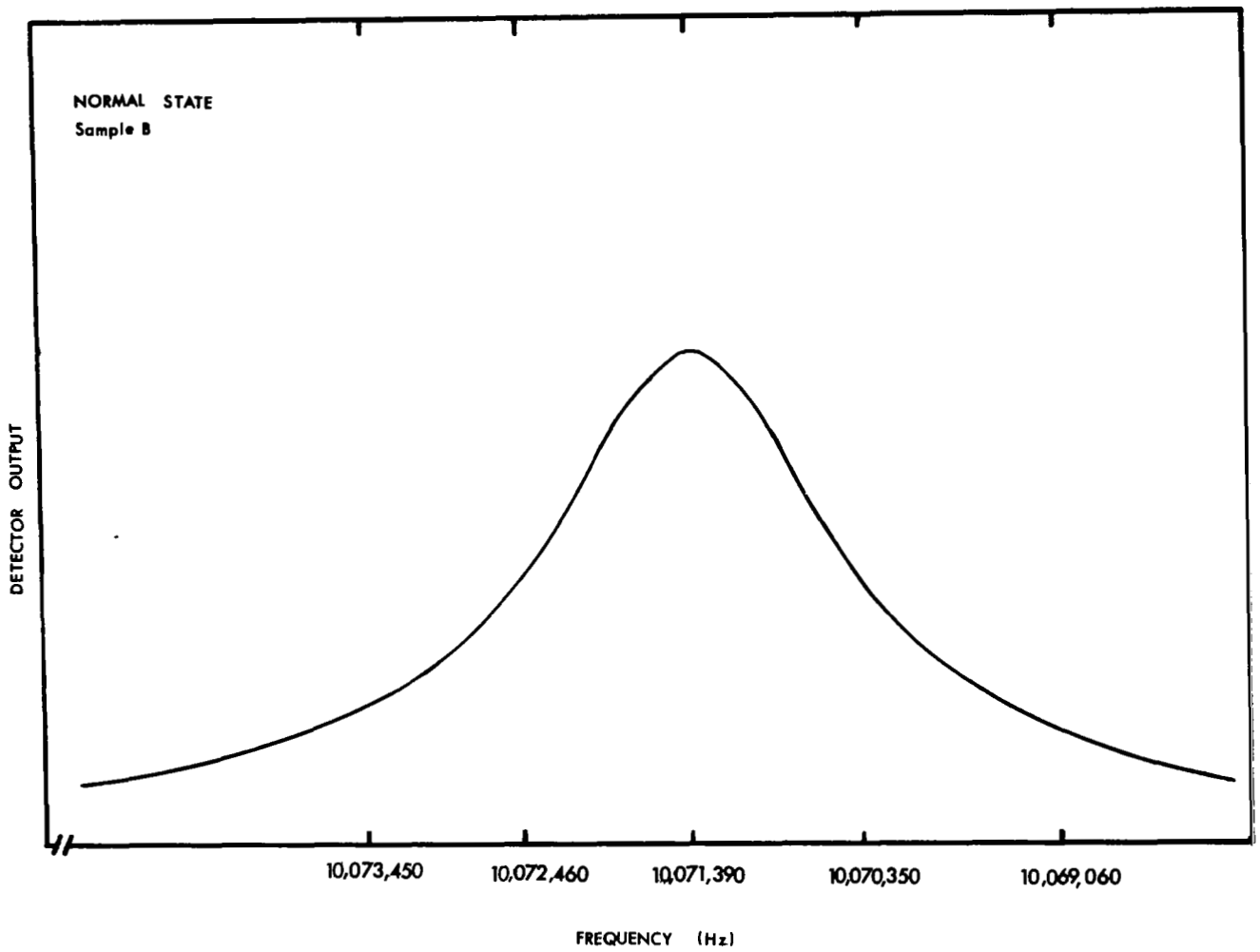

Figure 30. Detector output (arbitrary scale) vs. frequency in the normal state for C_{44} transverse waves in Sample B at 4 K.